Research Square

Preprints are preliminary reports that have not undergone peer review.
They should not be considered conclusive, used to inform clinical practice,
or referenced by the media as validated information.

Exploring the antioxidant, anticancer, and cytotoxic effects of Caesalpinia digyna (Rottl.) fruit extracts along with GC-MS profiling: Combined in vitro and computational modeling studies

Kaniz Fatema
Comilla University
Md. Anamul Haque
Comilla University
Jinat Fatema Sharna
Comilla University
Md Abdul Majed Patwary
Comilla University
Md. Najem Uddin
Bangladesh Council of Scientific and Industrial Research
Mohsin Kazi
King Saud University
Ashok Kumar
King Saud University
Nellore Bhanu Chandar
University of Kentucky
Chang-Guo Zhan
zhan@uky.edu

University of Kentucky

Article

Keywords: Caesalpinia digyna, GC-MS profiling, 1,3-Dihydroxyanthraquinone (C14), Anticancer, Molecular Docking, MD simulation

Posted Date: June 30th, 2025

DOI: https://doi.org/10.21203/rs.3.rs-6917913/v1

License: This work is licensed under a Creative Commons Attribution 4.0 International License.
Read Full License

Additional Declarations: No competing interests reported.

Version of Record: A version of this preprint was published at Scientific Reports on December 3rd, 2025. See the published version at https://doi.org/10.1038/s41598-025-29284-9.

Abstract

Background

Caesalpinia digyna Rottl. is an evergreen shrub traditionally used as an astringent, phthisis, antipyretic, nervine tonic, and diabetes remedy.

Aim

Our main goal is to determine the fruit extract's antioxidant, anticancer, and cytotoxic effects through *in vitro* and computational studies.

Methods

Firstly, methanol extract was prepared, and the fractionation was carried out using petroleum ether, dichloromethane, ethyl acetate, and distilled water. Preliminary screening was done using qualitative techniques, while Folin-Ciocalteu and $AlCl_3$ techniques were used to measure the total phenol (TPC) and flavonoid content (TFC), respectively. The total antioxidant capacity, DPPH scavenging, and Fe^{3+} reducing power were used to calculate the antioxidant activity using a spectrophotometric technique. Besides, Trypan Blue Exclusion and MTT methods were used to measure cytotoxic and anticancer activities against Vero and different cancer cell lines. GC-MS profiling was also carried out to identify the plant's phytochemicals.

Results

The phytochemical screening revealed various phytoconstituents, and the GC-MS analysis discovered 40 bioactive compounds in the ethyl acetate extract (ECDF). The ECDF showed the highest TPC (258.16 ± 4.84 mg GAE/g), TFC (174.25 ± 8.33 mg QCE/g), and potent antioxidant capacity. In the *in vitro* anticancer and cytotoxicity studies, the lowest viability was shown by the ECDF at doses of 800 µg/mL against lung cancer (43.97 ± 2.95%) and Vero cell (53.58 ± 3.20%) lines. Besides, ECDF extract has strong anticancer effects against breast cancer cell lines MCF-7 and MDA-MB-231 (IC_{50}: 23.53 ± 1.61 and 15.57 ± 3.74 µg/mL). Moreover, the docking results showed that the selected compounds have a strong binding affinity for various proteins and bind to amino acid residues via hydrogen bonds and non-covalent and Van Der Waals interactions. Molecular dynamics simulations revealed that the 1,3-dihydroxyanthraquinone (C14) compound forms stable complexes with respective proteins.

Conclusion

Our findings suggest that *C. digyna* fruit extracts might be a potential source for discovering cancer medicine. However, further analysis is required to isolate and identify the compounds responsible for these effects.

1. Introduction

Natural medicines derived from plants, animals, microorganisms, and marine organisms have been used by humans to treat and prevent diseases since the dawn of time. According to fossil records, people have been using plants as medicines for at least 60,000 years [1].

Oxidative stress originates from an imbalance between bodily antioxidants and pro-oxidants, which generates hazardous radical species that seek stability by electron pairing with cellular macromolecules, damaging DNA, protein, lipids, and carbohydrates [2]. As a result of oxidative stress, cells can become damaged or die, which speeds up the aging process and contributes to a wide range of degenerative diseases and conditions. These include neurological disorders, Alzheimer's disease, cancer, cardiovascular disease, cataracts, atherosclerosis, and diabetes. Antioxidants are chemicals that slow down or stop a target molecule from suffering oxidative damage. Nucleic acids, proteins, carbohydrates, and lipids are all prevented from oxidizing by antioxidants [3]. Antioxidants serve as scavengers, reducing cell and tissue damage by preventing or delaying oxidation. Antioxidants neutralize free radicals before they can damage cells by giving up a hydrogen atom to the reactive radical intermediate [3].

Cancer is the second-largest cause of mortality globally, accounting for an expected 9.7 million deaths and 20 million new cases in 2022. Based on estimates, one in five men and women will have cancer in their lifetime, while one in nine men and one in twelve women will pass away from it [4, 5]. It is distinguished by aberrant division of cells and proliferation brought on by an interruption in the molecular signals controlling these processes [6]. Lung cancer was the leading cause of cancer-related mortality in 2022, with a projected 1.8 million deaths (18.7%) and around 2.5 million new cases, or one in eight malignancies globally (12.4% of all cancers) [5]. Breast cancer is the second-most prevalent form of cancer globally, accounting for an expected 2.3 million new cases in 2022, or 11.6% of all new cancer diagnoses, and is the leading cause of death (6.9%). It is also known as the most common and potentially lethal disease in women [5, 7]. Worldwide, kidney or renal cancer (including renal pelvis) ranked 16th among all cancers with 431288 new cases (2.2% of all sites) and 14th with 179368 new deaths (1.8% of all sites) [8].

80% of people rely on plants for their basic medical needs. The discovery of clinically significant anti-cancer medications like Vincristine, Vinblastine, Taxol, Etoposides, and Camptothecin, which can stop the growth of cancer cells by regulating apoptosis and autophagic pathways, was made possible by the screening of up to 35,000 plant species for anti-cancer properties. However, multidrug resistance and the harmful effects of existing chemotherapeutic medicines on other non-target tissues make it imperative to discover novel bioactive compounds with fewer side effects and more efficacy [6].

Caesalpinia (C.) digyna Rottl. is an evergreen and perennial shrub of the Fabaceae family, traditionally used as an astringent, phthisis, antipyretic, nervine tonic, and for diabetes. It is usually distributed in India, Nepal, Burma, Myanmar, China, and Bangladesh [9]. The root extract has significant antioxidant, antiviral, anticancer, anti-obesity, antiulcerogenic, antiarthritic, antitubercular, hepatoprotective, antiarrhythmic, burn wound healing, radioprotective, as well as trypanocidal activities [10], [11]. The methanolic extract of leaves of *C. digyna* has also shown analgesic, antipyretic, anti-inflammatory, and thrombolytic effects [12].

To the best of our knowledge, this is the first study of *C. digyna* fruits for the phytochemical and pharmacological activities coupled with the computer-assisted approach. This research aims at phytochemical screening and GC-MS analysis, as well as investigating the in vitro antioxidant, anticancer, and cytotoxic effects of fruit extracts.

2. Materials & Methods

2.1 Fruits Collection and Identification

Caesalpinia digyna fruits were collected in February 2022 from the Cumilla Hill Tract (23°25'07.1"N 91°07'51.1" E), Cumilla, Bangladesh (Fig. 1). The Bangladesh National Herbarium's Mirpur, Dhaka, taxonomist identified the fruits. Then, under the reference number DACB-87200, a voucher specimen was deposited. The dried fruits were cleaned well, pulverized into a coarse powder using a grinding mill, and stored at room temperature for experimental analysis.

2.2 Chemicals and Reagents

Analytical-grade chemicals and reagents were used in this research. Methanol, Mayer’s reagent, Lead acetate solution, 2,2-diphenyl-1-picrylhydrazyl (DPPH), and Folin-Ciocalteu reagent were bought from Merck (Darmstadt, Germany). The Sigma Chemicals Co. (St. MO, USA) provided Potassium ferricyanide, Trichloroacetic acid, Dimethyl sulfoxide, Helium, Doxorubicin hydrochloride, and Dimethyl Sulfoxide (DMSO). In addition, MTT (3-(4,5-dimethyl-thiazol-2-yl)-2,5-diphenyltetrazolium bromide), Trypan blue (0.4%), Antibiotic (penicillin/streptomycin) (100X), Phosphate-buffered saline (PBS) (pH = 7.2, 1X), Trypsin-EDTA (0.25%, 1X), Fetal bovine serum (FBS), DMEM/F-12 (Dulbecco’s Minimum Essential Medium) (1X), T-25 and T-75 flasks, 96-well plates, serological pipettes, and pipette tips were purchased from Gibco, Invitrogen (Eugene, OR, USA).

2.3 Cell Lines

Human lung adenocarcinoma cell line (A-549) and Vero (ATCC-CCL-81 normal kidney epithelial cell line) were collected from the National Centre for Cell Science (NCCS) in Pune, India. Besides, the two human breast cancer cell lines, MCF-7 and MDA-MB-231 (human breast carcinoma, ER-, tumorigenic, and invasive cell line), were utilized in the anticancer assay. These cells were cultivated in a 75 cm^2 tissue

culture flask using DMEM media supplemented with 10% FBS, 1% penicillin/streptomycin, and 5% CO_2 at 37 ºC.

2.4 Extraction and Fractionation of Fruits

The amber-colored extraction containers were filled with roughly 500 grams of powdered fruit, which were then soaked in 2.5 L of methanol. Over 14 days, the bottles were shaken and stirred occasionally. After filtering the entire mixture via Whatman (no.1) filter paper, a rotary evaporator was used to extract the solvent. The methanolic fruit extract was given a dark chocolate brown, gummy, and sticky concentration (30g). After that, 10 g was kept in a glass vial, and the remaining 20 g was gradually fractionated four times using the Kupchan process [13]. Each time, weigh 5 g with petroleum ether, dichloromethane, and ethyl acetate after dissolving the gummy extract in methanol and adding water. Later, four fractions were dried to obtain petroleum ether (PCDF, 4.02g), dichloromethane (DCDF, 4.95g), ethyl acetate (ECDF, 5.02g), and water (WCDF, 6.01g) fractions of *C. digyna*. In the refrigerator, these were kept in sealed containers (4◦ applications).

2.5 Preliminary Phytochemical Screening

Using established phytochemical screening procedures, freshly made fruit extract of methanolic extract of *C. digyna* fruit (MCDF), PCDF (Petroleum extract of *C. digyna* fruit), DCDF Dichloromethane extract of *C. digyna* fruit), ECDF (Ethyl acetate extract of *C. digyna* fruit) and WCDF (Water extract of *C. digyna* fruit) were examined for alkaloids, flavonoids, saponins, glycosides, tannins, resins, steroids, anthraquinones, and phlobatanins [14].

2.6 GC-MS Analysis

2.6.1 Sample Preparation

The ethyl acetate fruit extract was transferred to a GC-MS vial and dried using nitrogen air. The completely dried vial was derivatized using 100 µL methoxylamine hydrochloride in pyridine (1:10). Then, this mixture was vortexed for 10 min and left for 16 hours at room temperature. 100 µL of derivatizing agent BSTFA + TMCS was added to the vial, vortexed for 10 min, and kept at 60°C on the hot plate. Finally, 1 µL of this solution was injected into the GC-MS.

2.6.2 Instrumental Analysis

An Agilent GC 7890A and a triple-axis detector 5975 C single quadrupole mass spectrometer were used for GC-MS analysis. High-purity helium was used as the gas carrier in the Agilent HP 5MS chromatographic column (30 m × 0.25 mm × 0.25 µm film thickness) at a flow rate of 1 mL/min. In addition to having a splitless injector at 20:1, the injector had a temperature of 250°C. The quad temperature was 150°C, and the MS source temperature was set at 230°C. First, the oven was set to 40°C (held for 1 minute), and then it was raised to 300°C at 10°C min^{-1} (kept for 5 minutes). One microliter was used for injection, the solvent delay was seven minutes, and the scan range was set between 40 and 600 mass ranges at 70 eV electron energy. After that, the spectra were compared to

those of the National Institute of Standards and Technology Library (NIST 2008) to identify the unknown chemicals. The entire time needed to analyze the sample was thirty-two minutes [15], [16].

2.7 Quantitative Analysis of C. digyna Fruit Extracts

2.7.1 Determination of Total Phenol Content (TPC)

Total phenolic content was determined using the modified Folin-Ciocalteu technique, which was established by Wolfe *et al.* [17]. 1 mL of the extracts (1 mg/mL) or gallic acid (GA) (50–400 µg/mL) solution was combined with 1 mL of Folin-Ciocalteu reagent. After 5 minutes, 10 mL of Na_2CO_3 (7%) solution and 13 mL deionized water were added and incubated for 90 minutes at 23°C. Using a double-beam UV-visible spectrophotometer, absorbance at 750 nm was measured. The absorbance of GA was used to create a regression equation ($y = 0.0052x + 0.8009$; $R^2 = 0.9827$), from which the TAC was determined as mg/g GA equivalent [18].

2.7.2 Determination of Total Flavonoid Content (TFC)

The flavonoid content was measured spectrophotometrically using the $AlCl_3$ technique established by Brighente *et al.* [19]. 1 mL (0.5 mg/mL) of the extracts or 1 mL (125 to 1000 µg/mL) standard (Quercetin, QC) solution was combined with 0.5 mL of $AlCl_3$ (2%) solution and 0.5 mL deionized water. Absorbance was measured at 430 nm following 15 minutes of incubation at 25 ^oC. Based on the absorbance of QC, a regression equation ($y = 0.0024x + 0.4109$; $R^2 = 0.987$) was created, and the TFC was calculated as mg/g of QC equivalent [20].

2.7.3 In vitro Antioxidant Effect

2.7.3.1 Determination of Total Antioxidant Content (TAC)

Total antioxidant capacity (TAC) was measured spectrophotometrically using the phosphormolybdenum assay established by Prieto *et al.* [21]. In test tubes, 0.3 mL ascorbic acid (AA) (25 to 400 µg/mL) or 0.3 mL of extracts (100 µg/mL) were combined with 3 mL of the reagent solution (0.6 mM H_2SO_4, 28 mM Na_3PO_4, and 4 mM $(NH_4)_2MoO_2$ in deionized water). The mixture was heated at 95 ^oC for 90 minutes in a water bath. Absorbance was measured at 695 nm wavelength after cooling in tap water. TAC was calculated as mg/g of ascorbic acid (AA) equivalent using the regression equation ($y = 0.0074x + 0.9221$; $R^2 = 0.9889$) developed from the absorbance value of AA, which served as the reference compound [22].

2.7.3.2 DPPH Radical Scavenging Effect

The DPPH radical scavenging test measures free radical-scavenging potential reported by Blois [23] and Demarchelier *et al.* [24]. DPPH gives a violet or purple color in an ethanol solution, in which antioxidants turn yellow. The 0.1 mM DPPH in ethanol solution was added to 6.25–400 µg/mL of extract in methanol. Vortexed and left for 30 minutes at room temperature in the dark. Absorbance at 517 nm was measured.

AA was the standard. To calculate the percentage of DPPH radical scavenging activity, the following formula was utilized:

$$\%\ \mathbf{DPPH\ radical\ scavenging\ activity} = \frac{\mathbf{Absorbance\ of\ control} - \mathbf{Absorbance\ of\ extract}}{\mathbf{Absorbance\ of\ control}} \times 100$$

The IC_{50} was calculated by plotting percent inhibition vs concentration. Three times for each concentration [25].

2.7.3.3 Ferric Reducing Power Assay

The ferric-reducing antioxidant capacity of the samples was determined using Oyaizu's technique [26]. 2.5 mL of different concentrations of samples/standard solutions (12.5–400 µg/ml), 2.5 mL of potassium buffer (0.2 M), and 2.5 mL of potassium ferricyanide, $[K_3Fe(CN)_6]$ solution, were added to the test tubes. The reaction mixtures were incubated at 50°C for 20 minutes to complete the reaction. After that, 2.5 mL of a 10% trichloroacetic acid (TCA) solution was added to the test tubes. 2.5 mL of supernatant was taken from the test tubes and mixed with 2.5 mL of distilled water and 0.5 mL of 0.1% ferric chloride solution after centrifuging the entire mixture at 3000 rpm for 10 minutes. Then, absorbance was measured at 700 nm against a blank. Then, the EC_{50} value of each extract and the standard compound were found [25].

2.8 In Vitro Anticancer and Cytotoxicity Test

2.8.1 Lung Cancer Cell Line (A-549) and Vero Cell Line

The cytotoxic effect was investigated on the A-549 cell line, a type of lung cancer cell, and the Vero cell line (ATCC- CCL-81), derived from normal kidney epithelial cells, utilizing a slightly modified variation of the Trypan Blue Exclusion method [27]. These cells were cultivated in flasks, utilizing the media described by Khan *et al.* [28], under controlled conditions of 37°C temperature and a 5% (v/v) concentration of CO_2. The negative control group is comprised of samples containing 0.6% DMSO. Comparative analyses were conducted on the treatment groups, consisting of the standard drug doxorubicin (DR) at a concentration of 1 µg/mL and various extracts. Additionally, a vehicle group (DMSO), serving as the negative control, was included in the analysis. The A-549 and Vero cells were subdivided the day before they were utilized in the assays. The recently produced concentrations of (200 µg/mL, 400 µg/mL, and 800 µg/mL) of DCDF, ECDF, and WCDF fractions were introduced into cultured T-flasks containing approximately 2.5×10^6 cells/well (for A-549) and 2.3×10^6 cells/well (for Vero cell) a day before the commencement of the experiment. The cells were harvested utilizing trypsin at a concentration of 0.5% following a 24-hour incubation period. The automated cell counter (LUNA-II™, South Korea) was employed to ascertain the number of deceased cells, utilizing a 0.4% w/v concentration of Trypan blue. The calculation of the percentage of cell viability was performed utilizing the following mathematical formula:

$$\%\ \mathbf{of\ cell\ viability} = \frac{\mathbf{Concentration\ of\ live\ cells}}{\mathbf{Total\ concentration\ of\ cells}} \times 100 \ldots\ldots\ldots \mathbf{(1)}$$

2.8.2 Breast Cancer Cell Lines (MCF-7 and MDA-MB-231)

The degree of cellular cytotoxicity induced by ECDF extract was evaluated by measuring the reaction of mitochondrial dehydrogenase of live cell enzymes with yellow MTT (3-(4, 5-dimethylthiazolyl-2)-2,5-diphenyltetrazolium bromide) to purple formazan crystals. Briefly, complete cell growth media was used to plate breast cancer cells in 96-well plates (2×10^3 cells/well), and the cells were then incubated for 24 hours at 37°C in a humidified environment with 5% CO_2. After that, the cell media was swapped out for a cell growth medium that had 5% FBS (5% medium) and various formulation concentrations, including 3.9, 7.8, 15.6, 31.25, 62.5, 125, 250, and 500 µg/mL, along with a control (without any formulation). Following a 72-hour incubation period, 100 µL/well of MTT solution (0.5 mg/mL, in PBS) was added to all test and control wells to replace the medium, and the mixture was then incubated for an additional three hours at 37°C. The purple formazan crystals that had developed at the bottom of the wells were then dissolved by replacing the MTT solution with 100 µL of isopropanol per well and shaking the wells for at least two hours at room temperature. A Bio-Tek microplate reader (ELX 800; Bio-Tek Instruments, Winooski, VT, USA) was then used to measure the color intensity in the wells at 549 nm. The viability percentage was computed after the findings were examined in triplicate. As previously mentioned, the data are displayed as the percentages of cell viability in the test wells relative to the control group [7], [29].

2.9 Computational Modeling Studies

2.9.1 Ligand and protein preparation, docking, and nonbonding interactions

The structure of fifteen major compounds from ethyl acetate fraction, namely Trimethylsilyl ether of glycerol (C1, PubChem CID: 522285), Benzoic acid, 2,5-dihydroxy-(C2, PubChem CID: 3469), Xylonic acid, 2,3,4-tris-O-(trimethylsilyl)-, .delta.-lactone-(C3, PubChem CID: 523413), Mannonic acid, 2,3,5,6-tetrakis-O-(trimethylsilyl)-, lactone-(C4, PubChem CID: 523382), Fructofuranoside, methyl 1,3,4,6-tetrakis-O-(trimethylsilyl)-, .alpha.-D-(C5, PubChem CID: 612554), Trimethylsilyl-meso-inositol (C6, PubChem CID: 520232), Beta-D-Galactofuranose, 1,2,3,5,6-pentakis-O-(trimethylsilyl)- (C7, PubChem CID: 6432661), 1-Methylbenzo[f]quinolin-3-ol (C8, PubChem CID: 336100), 1-Pentene, 1,3-diphenyl-1-(trimethylsilyloxy)-(C9, PubChem CID: 5378122), Ethyl 3,4,5-tris[(trimethylsilyl)oxy]benzoate (C10, PubChem CID: 553710), Acrylic acid, 2,3-bis[(trimethylsilyl)oxy]-, trimethylsilyl ester (C11, PubChem CID: 5366618), Estra-1,3,5(10),6-tetraen-17-one, 3-[(trimethylsilyl)oxy]-, O-methyloxime (C12, PubChem CID: 20845840), 1,8-Dihydroxyanthraquinone, O,O'-bis(trimethylsilyl)-(C13, PubChem CID: 632786), 1,3-Dihydroxyanthraquinone (C14, PubChem CID: 196978), Guaicol-.beta.-d-glucopyranoside, pentakis(O-trimethylsilyl)-(C15, PubChem CID: 553905) was drawn by ChemDraw software (Fig. 2). Then, using the program Gaussian 09W edition D.01 and density functional theory (DFT), in addition to B3LYP hybrid functionals, and Pople's 6-31G+(d, p) basis set, geometry optimization was carried out [30].

The PDB files of three-dimensional structures of the proteins were downloaded from the RCSB Protein Data Bank (https://www.rcsb.org/) [31], including the KEAP1 protein (Human self-inducible nitric oxide

synthase, PDB: 4IFJ, resolution: 1.80 Å) [32], vascular endothelial growth factor receptor2 (VEGFR2) kinase proteins (PDB: 3VHE, resolution: 1.55 Å) [33] and (PDB: 2XIR, resolution: 1.50 Å) [34], and human epidermal growth factor2 (HER2) protein (PDB: 3PP0, resolution: 2.25 Å) [35]. The Protein Preparation Wizard [36] of the Maestro-V13.0 in the Schrödinger software suite [37] was used to clean the undesired chain, heteroatoms, water molecules, and co-crystallized ligand molecules. Finally, for each ligand-protein pair, cavity detection-guided blind docking was carried out using the CB-Dock 2 [38] against the protein (associated with PDB 4IFJ, 3VHE, 2XIR, or 3PP0). The cavity volume ($Å^3$) was 1217, 760, 735, and 4432 for 4IFJ, 3VHE, 2XIR, and 3PP0, respectively. The obtained ligand-protein complex was saved to a PDB file, which was loaded into the BIOVIA Discovery Studio 2021 for the non-bonding interaction calculations.

2.10 Molecular Dynamics (MD) Simulations

MD simulation on each ligand-protein complex was performed for 400 ns by utilizing the AMBER20 program (Sander module in the Amber Tools) [39] to validate the stability of the complex. The docked binding complex with ligand C14 was energy-minimized using the AMBER ff19SB force field for protein and the general AMBER force field (GAFF2) for ligand C14 using the Amber20 program [39]. The restricted electrostatic potential (RESP) charges are used for C14. The RESP charges were determined by using the Gaussian16 program [40] by optimizing the C14 geometry (**Figure S1)**, calculating the electrostatic potential at the B3LYP/6–31 + G* level, and then fitting the QM-calculated electrostatic potential to the RESP [41]. The docked protein-C14 binding structure was soaked with TIP3P water molecules [42] in an orthorhombic box with a minimum solute wall distance of 12 Å. The overall charge of the system was neutralized by adding counter ions. The energy minimization for every protein-C14 complex was initially done with the steepest descent method for 2,500 steps, followed by the conjugate gradient method until convergence. After minimizing energy, the positioning restraints for each complex were equilibrated using an NVT ensemble (100 ps) and a normal constant pressure-temperature (NPT) ensemble (100 ps). Finally, a 400 ns MD simulation was performed, without position restraints, for each complex with Berendsen Barostat (pressure) and Langevin thermostat (temperature) controls. Additionally, Molecular Mechanics-Generalized Born Surface Area (MM-GBSA) binding free energy calculations were performed using 1000 snapshots of the MD trajectory during the final 100 ns to estimate the binding free energy of ligand C14 with the protein.

2.11 Statistical Analysis

All data were analyzed by using the GraphPad Prism 10.2 software (GraphPad Software, La Jolla, CA). The one-way analysis of variance (ANOVA) was used to compare the changes of all groups with the control group. A difference was considered significant when $p < 0.05$ (* $p < 0.05$, ** $p < 0.01$, *** $p < 0.001$, and **** $p < 0.0001$).

3. Results

3.1 Phytochemical Screening Test

The phytochemical analysis revealed a wide range of compounds, such as alkaloids, flavonoids, saponins, glycosides, tannins, resins, steroids, and anthraquinone. **Table S1** shows that these secondary metabolites were present in ECDF, WCDF, DCDF, MCDF, and PCDF extracts of *C. digyna* fruit. Only glycosides are absent from the PCDF extract.

3.2 GC-MS Analysis

In the ethyl acetate extract of *C. digyna*, Gas chromatography-mass spectra revealed 40 peaks, indicating the presence of 40 distinct phytochemical components (Fig. 3). The 40 phytocompounds were described and identified by comparing the constituents' mass spectra to the NIST library. Here, Trimethylsilyl ether of glycerol (C1) was the first bioactive compound with a retention time of 11.21 min, and it has antioxidant, antibacterial, antifungal, nematocidal, and pesticidal properties [43]. However, 2-(Acetoxymethyl)-3-(methoxycarbonyl) biphenylene was the last phytochemical with a retention time of 30.54 min and a biphenylene class (**Table S2**). Overall, these phytoconstituents are classified as ethers, alcohols, aldehydes, ketones, esters, etc.

3.3 Quantitative Analysis

3.3.1 Total Phenol Content (TPC) and Total Flavonoid Content (TFC)

From the data in Table 1, ECDF exhibited the maximum level of TPC (258.16 ± 4.84 mg GAE/g) and TFC (174.25 ± 8.33 mg QCE/g), whereas PCDF showed the minimum level of 87.01 ± 1.11 mg GAE/g and 38.14 ± 12.73 mg QCE/g, respectively. The order among the extracts was ECDF > WCDF > DCDF > MCDF > PCDF for TPC and TFC.

Table 1
TPC, TFC, TAC, IC_{50} (DPPH), EC_{50} (FRPT) *C. digyna* fruit extracts.

Parameters	Standard	Extracts of *C. digyna*				
	AA	MCDF	PCDF	DCDF	ECDF	WCDF
TPC (mg/g) equivalent of GA	-	204.96 ± 4.00	87.01 ± 1.11	215.85 ± 7.28	258.16 ± 4.84	233.80 ± 5.88
TFC (mg/g) equivalent of QC	-	88.14 ± 4.81	38.14 ± 12.73	115.92 ± 8.33	174.25 ± 8.33	146.47 ± 12.73
TAC (mg/g) equivalent of AA	-	220.77 ± 6.19	166.72 ± 6.19	245.09 ± 10.20	303.20 ± 8.11	278.88 ± 10.73
IC_{50} (DPPH)	5.27 ± 0.94	57.9 ± 6.87	119.51 ± 6.89	41.61 ± 2.66	10.96 ± 2.32	22.55 ± 2.58
EC_{50} (FRPT)	9.76 ± 1.35	39.64 ± 2.59	68.30 ± 2.62	23.52 ± 2.09	12.50 ± 2.44	15.45 ± 1.87

Data are the mean **±** SD, n = 3. **TPC**: Total phenol content, **TFC**: Total flavonoid content, **TAC**: Total antioxidant content, **IC**: Inhibitory concentration, **EC**: Effective concentration, **GA**: Gallic acid, **QC**: Quercetin, **AA**: Ascorbic acid, **MCDF**: Methanolic extract of *C. digyna* fruit, **PCDF**: Petroleum extract of *C. digyna* fruit, **DCDF**: Dichloromethane extract of *C. digyna* fruit, **ECDF**: Ethyl acetate extract of *C. digyna* fruit, **WCDF**: Water extract of *C. digyna* fruit.

3.3.2 In Vitro Antioxidant Effects

3.3.2.1 Total Antioxidant Content (TAC)

Herein, ECDF had the greatest TAC among the extracts (303.20 ± 8.11 mg AAE/g). In contrast, WCDF, DCDF, MCDF, and PCDF had 278.88 ± 10.73 mg/g, 245.09 ± 10.20 mg/g, 220.77 ± 6.19 mg/g, and 166.72 ± 6.19 mg/g equivalent of AA, respectively (Table 1).

3.3.2.2 DPPH Radical Scavenging Effect

In a manner that was dependent on concentration, both the extracts and the AA had an inhibiting effect on the DPPH radicals. Table 1 depicts that the inhibitory impact of AA, ECDF, WCDF, DCDF, and MCDF was considerable, with IC_{50} values of 5.27 ± 0.94 µg/mL, 10.96 ± 2.32 µg/mL, 22.55 ± 2.58 µg/mL, 41.61 ± 2.66 µg/mL, and 57.9 ± 6.87 µg/mL, respectively. AA > ECDF > WCDF > DCDF > MCDF > PCDF had the greatest DPPH radical inhibitory effect.

3.3.2.3 Ferric Reducing Power Test (FRPT)

The ability of AA, MCDF, PCDF, DCDF, ECDF, and WCDF to reduce ferric ions in vitro is shown in Table 1. Here, AA showed the lowest EC_{50} (9.76 ± 1.35 µg/mL), then ECDF (12.89 ± 1.68 µg/mL), followed by WCDF, DCDF, MCDF, and PCDF extracts. The antioxidant power was greater when the EC_{50} value was lower.

3.4 Computational Modeling Analysis

3.4.1 Computational Studies against Antioxidant Protein (4IFJ)

Tables 2 and S3 and **Figure S2** show the results of molecular docking experiments and non-bonding interaction investigations for antioxidant activity. Compound C12 had the best binding score (-9.3 kcal/mol) with the receptor protein 4IFJ compared to other drug candidates. In contrast, a less favorable binding score (-4.5 kcal/mol) of compound C7 shows that C7 has only a very low binding affinity to the protein. Non-covalent interactions are crucial for preserving drug stability, altering binding affinities, and increasing the effectiveness of medications [44]. In our study, all compounds have hydrogen bonds with different amino acids except for compounds C1, C7, and C9. Besides, all compounds have hydrophobic interactions with several amino acid residues except for compounds AA, C3, and C11. Moreover, Van Der Waals interactions are found in all drug candidates with different amino acid residues.

Table 2
Docking simulation with antioxidant protein (PDB ID: 4IFJ) including binding affinity, H-bonds, hydrophobic bonds, and Van Der Waals interactions.

ID	BA (kcal/mol)	Hydrogen bonds (A^0)	Hydrophobic bonds	Van Der Waals interactions
AA	**-6.3**	VAL512 (2.58), ILE559 (2.24), VAL465 (2.26), ILE416 (2.58), VAL463 (2.67), VAL604 (2.69), GLY511 (3.59), GLY558 (3.28)	-	VAL606, GLY367, GLY605, ALA366, LEU365, GLY464, GLY417
C8	**-8.4**	ALA510 (2.98), GLY509	**PA**: ALA366, VAL606	ILE559, GLY462, VAL563, GLY464, VAL465, VAL512, GLY511, GLY603, GLY364, LEU365, VAL604, GLY605, GLY367
C12	**-9.3**	ARG415 (2.88)	**A**: ALA366	ALA556, ALA510, GLY511, ILE416, GLY464, GLY417, VAL463, ILE559, VAL512, VAL465, THR560, VAL418, VAL369, CYS513, VAL608, ALA466, VAL514, ALA607, VAL467, CYS368, GLY419, VAL420, VAL606, GLY367, GLT605, VAL604, LEU365, GLY558, GLY364, GLY603, LEU557, GLY462, GLY509
C14	**-8.7**	GLY367 (2.98), GLY367 (1.96), VAL465 (2.92), VAL512 (2.27), ALA366 (3.23), GLY464 (3.52), GLY605 (3.61)	**PA**: ALA366, ALA366	ILE559, ALA510, VAL463, LEU365, VAL604, VAL606

AA: Ascorbic acid, **BA**: Binding affinity, **A**: Alkyl, **PA**: π-alkyl

3.5 In Vitro Anticancer Tests

3.5.1 Lung Cancer Cell (A-549) Line by Trypan Blue Exclusion Method

A-549 cells are a widely accepted cell line for lung cancer studies. Standard drug doxorubicin (DR) (1 µg/mL) showed 62.04 ± 0.99% viability against the lung cancer cells. The control group (DMSO) had almost no effect as expected, but the ECDF, WCDF, and DCDF had a significant impact with 43.97 ± 2.95%, 65.03 ± 3.57%, and 63.24 ± 2.36% viability at a concentration of 800 µg/mL on A-549 cells. All the fractions showed an inhibitory effect in a dose-dependent manner (**Table S4**, Figs. 4 and 5).

3.5.2 Computational Studies against Lung Cancer Protein (3VHE)

Tables 3 and S5 and **Figure S3** show the results of molecular docking and non-bonding interaction investigations against the lung cancer protein. The C14 had the best binding score (-9.2 kcal/mol) compared to the other compounds. In contrast, the DR depicts a -9.1 kcal/mol binding score with the receptor protein 3VHE. In our study, C14 has two H-bonds with CYS919 and LYS920 amino acids at distances of 1.91 Å and 1.93 Å, respectively. On the other hand, the standard drug (DR) contains six H bonds and three hydrophobic interactions, such as π-anion, alkyl, and π-alkyl interactions with numerous amino acids. Herein, only C3 and C4 compounds have no hydrophobic interactions, but all the compounds have Van Der Waals interactions with different amino acids.

Table 3
Docking simulation with lung cancer protein (PDB ID: 3VHE) including binding affinity, H-bonds, hydrophobic bonds, and Van Der Waals interactions.

ID	BA (kcal/mol)	Hydrogen bonds (A^0)	Hydrophobic bonds	Van Der Waals interactions
DR	**-9.1**	ARG1027 (2.66), GLU885 (2.48), GLU885 (3.00), ILE1025 (2.15), HIS1026 (3.25), ASP1046 (3.61)	**PAn**: ASP1046, ASP1046; **A**: LEU1049, LEU889, VAL899, CYS1045; **PA**: ILE888	GLU815, ASP814, LYS868, ALA881
C8	**-9.0**	CYS919 (1.90)	**PS**: VAL848, LEU1035; **PPTS**: PHE1047; **A**: LYS868, LEU889, VAL899, VAL916; **PA**: ALA866, LEU1035, LEU840, VAL848, ALA866, CYS919, LEU1035	GLY922, PHE918, LYS920, GLU917, VAL926, VAL899
C12	**-8.6**	CYS1045 (3.34), ILE1044 (3.32), ILE1044 (3.32)	**A**: ILE888, LEU1019, ILE888, LEU889, ILE892; **PA**: HIS1026, CYS817, ILE888	VAL899, VAL898, ASP1046, ILE892, ARG1027, ILE1025, ASP814, GLU885, ALA881
C14	**-9.2**	CYS919 (1.91), LYS920 (1.93)	**PS**: LEU840, LEU840, VAL848, LEU1035, LEU1035; **PPTS**: PHE1047; **PA**: VAL848, ALA866, ALA866	VAL899, VAL916, GLU917, PHE918, PHE921, GLY922, ASN923, GLY841, LYS868

DR: Doxorubicin, **BA**: Binding affinity, **A**: Alkyl, **PA**: π-alkyl, **PAn**: π-anion, **PS**: π-σ, **PPTS**: π-π-T shaped

3.5.3 Vero Cell Line by Trypan Blue Exclusion Method

Three extracts (DCDF, ECDF, WCDF) were tested for cytotoxicity using the Trypan Blue Exclusion method on Vero cells, with DR as a positive control group. The negative control group (DMSO) had almost no effect, but the ECDF (800 µg/mL) and WCDF (800 µg/mL) had significant effects with 53.58 ± 3.20% and

56.68 ± 3.98% viability of Vero cells. In addition, the DR showed 68.79 ± 1.27% viability of renal cells. All the fractions showed inhibitory effects in a dose-dependent manner (**Table S6**, Figs. 6 and 7).

3.5.4 Computational Studies against Renal Protein (2XIR)

Tables 4 and S7 and **Figure S4** display the outcomes of the docking simulation and non-bonding contacts for the renal protein 2XIR. In our research, DR displayed the best binding score (-11.0 kcal/mol) with the protein and followed by C14 (-8.8 kcal/mol) > C8 (-8.7 kcal/mol) > C12 (-8.0 kcal/mol) > C13 (-7.0 kcal/mol) > C9 (-6.9 kcal/mol) > C15 (-6.8 kcal/mol) > C11 (-6.7 kcal/mol) > C3 (-6.3 kcal/mol) > C10 (-6.1 kcal/mol) > C2 (-6.0 kcal/mol) > C4 (-5.9 kcal/mol) > C6 (-5.4 kcal/mol) > C5 (-5.1 kcal/mol) > C7 (-5.0 kcal/mol). This research demonstrated that all the selective compounds contain various hydrophobic interactions (except C1, C3, C4, and C5) with different amino acid residues. Here, DR, C1, C2, C3, C4, C5, C6, C8, C10, C11, C12, and C14 have H bonds, and all compounds contain Van Der Waals bonds with many amino acid residues.

Table 4
Docking simulation with renal cancer protein (PDB ID: 2XIR) including binding affinity, H-bonds, hydrophobic bonds, and Van Der Waals interactions.

ID	BA (kcal/mol)	Hydrogen bonds (A^0)	Hydrophobic bonds	Van Der Waals interactions
DR	**-11.0**	CYS817 (3.09), ILE1025 (2.48), ILE1025 (2.43), ASP1046 (2.88), GLY1048 (3.67)	**PC**: ARG1027, ARG1027, ARG1027; **PS**: HIS1026	CYS1045, LEU1019, ILE892, CYS1024, LYS868, GLU885, ILE888, HIS816
C8	**-8.7**	CYS919 (1.96)	**PC**: PHE918; **PS**: VAL848, LEU1035, LEU1035, LEU1035; **PPS**: PHE918; **A**: LEU840; **PA**: PHE1047, LEU840, ALA866, CYS919, ALA866	GLU917, VAL899, GLY922, VAL916
C12	**-8.0**	-	**A**: ILE888, CYS1024, CYS817, ILE888: **PA**: CYS1024	HIS816, ARG1027, ILE1025, ILE892, CYS1045, LEU1019, ASP1046
C14	**-8.8**	CYS919 (1.90)	**PS**: LEU840, LEU840, VAL848, LEU1035; **PPS**: PHE918; **PA**: ALA866, ALA866, LEU1035	VAL916, PHE1047, GLY922, GLU917, VAL899

DR: Doxorubicin, **BA**: Binding affinity, **A**: Alkyl, **PA**: π-alkyl, **PC**: π-cation, **PS**: π-σ, **PPS**: π-π-stacked

3.5.5 Breast Cancer Cell Lines (MCF-7 and MDA-MB-231) by MTT Assay

MCF-7 and MDA-MB-231 cell lines were used to test the impact of ECDF extract, and the results were compared to the control group, which consisted of cells stimulated with DMSO. Figures 8 and 9 represent the effect of ECDF extract on MCF-7 and MDA-MB-231 cell lines after a stimulation period of

72 h, respectively. The percentage of cell proliferation of ECDF was 9.17 ± 0.62% (MCF-7) and 21.09 ± 2.45% (MDA-MB-231) at the dose of 500 µg/mL, respectively, compared with controls (**Table S8**). The IC_{50} value of ECDF extract after 72 h post-stimulation was 23.53 ± 1.61 µg/mL for the MCF-7 cell line and 15.57 ± 3.74 µg/mL for the MDA-MB-231 cell line. The inhibition of tumor cells decreased in a dose-dependent manner after treatment with ECDF extract.

3.5.6 Computational Studies against Breast Cancer Protein (3PP0)

Table 5, S9, and **Figure S5** display the outcomes of the docking simulation and non-bonding contacts for the breast cancer protein 3PP0. The DR showed − 8.7 kcal/mol binding energy, whereas C14 and C8 exhibited a prominent effect with − 9.2 and − 9.0 kcal/mol binding energy, respectively. The remaining compounds showed binding affinity from − 4.3 to -7.7 kcal/mol. This research demonstrated that C14 showed one H-bond with ASP863 (2.05 Å), one π-alkyl interaction with nine amino acids, and eight Van Der Waals interactions with various amino acid residues. However, all compounds developed hydrophobic (except C7) and Van Der Waals interactions with various pocket residues.

Table 5
Docking simulation with breast cancer protein (PDB ID: 3PP0) including binding affinity, H-bonds, hydrophobic bonds, and Van Der Waals interactions.

ID	BA (kcal/mol)	Hydrogen bonds (A^0)	Hydrophobic bonds	Van Der Waals interactions
DR	**-8.7**	ARG811 (2.76), ARG849 (2.90), ARG849 (2.52), ALA730 (3.56), LYS921 (3.45)	**A**: LEU807; **PA**: PHE731, ALA730, PRO885	ASP808, CYS805, SER728, GLY729, ARG756, LYS883, LEU866, VAL884, TRP888
C8	**-9.0**	CYS805 (2.82)	**PS**: VAL734, VAL734, VAL734; **A**: ALA751, LEU726, LEU852; **PA**: LEU852, ALA751, LYS753	THR862, THR798, GLY804, ASP863, MET801
C12	**-7.7**	-	**A**: VAL734, VAL734, ALA751, ALA751, LYS753, LEU852, VAL734, LYS753, CYS805; **PA**: VAL734, CYS805	THR798, THR862, LEU726, ARG849, ASP808, SER728, GLY727, ASP863, PHE864, LEU796, LRU785
C14	**-9.2**	ASP863 (2.05)	**PA**: LEU726, VAL734, VAL734, ALA751, ALA751, LEU852, LEU852, LEU726, CYS805	SER783, THR798, MET801, GLY804, GLY729, SER728, ALA730, LYS753

DR: Doxorubicin, **BA**: Binding affinity, **A**: Alkyl, **PA**: π-alkyl, **PAn**: π-anion, **PS**: π-σ, **PPS**: π-π-stacked

3.6 MD Simulation Analysis

The dynamics simulation was performed to validate the binding process, structural characteristics, and flexibility of proteins in the presence of the C14 ligand [45]. To investigate the stability of the Cα atoms of proteins and ligands, the root mean square deviations (RMSD) were computed [46]. Herein, the average RMSD value of the Cα atoms of protein (black) is 1.5-2 Å (except breast cancer protein (3PP0) (2-3.5 Å), and the C14 ligand atom (blue) is 0.5-1 Å in Figs. 10**(b)-12(b)** suggesting that both protein and ligand are stable throughout the 400 ns. On the other hand, for the antioxidant protein, the hydrogen bond results **(**Fig. 10**(C) to (F))** represent four H-bonds with three amino acid residues, such as VAL418, VAL465, and ILE559, with distances ranging from 2.38 Å to 4.39 Å **(**Fig. 10**(A)).** Among them, O2(C14)-H(ILE559) is the most stable interaction (70%) compared to the others. In the case of lung cancer protein (3VHE) (Fig. 11**(A), (C), and (D))**, the C14 ligand has two strong H-bonds with GLU917 (100%) and CYS919 (98%) with distances of 1.76 Å and 1.98 Å, respectively. In addition, with the 2XIR protein, the C14 shows four moderates to weak H-bonds with four different amino acids, such as GLU70 (23%), HIE1026 (0%), CYS1045 (3%), and ASP1046 (0.1%) **(**Fig. 12**(C)** to **(F)).** This indicates that there might be some hydrophobic interactions, for example, π-alkyl, π-σ, and π-π-stacked, that contribute to holding the ligand in the binding site, as their RMSD value is low. Moreover, Figs. 13**(C)** and **(D)** of breast cancer protein (3PP0) depict a strong H-bond and a weak H-bond with the amino acid MET801 (99%) and THR862 (2%) at 3.43 Å and 1.99 Å, respectively (Fig. 15(A)).

The MM-GBSA approach was used to analyze the binding strength of proteins to C14 compounds by calculating the free energy of the protein-ligand interaction in the solvent environment. According to the results, which are shown in Table 6, the 3VHE-C14 complex had the most favorable binding free energy (-24.43 kcal/mol), followed by the 2XIR-C14 (-22.40 kcal/mol), 3PP0-C14 (-21.14 kcal/mol), and 4IFJ-C14 (-20.04 kcal/mol).

Table 6
For each complex, evenly taken 1000 snapshots of the MD trajectory during the last 100 ns, i.e., one snapshot for each 0.1 ns, for MM-GBSA binding free energy calculations. The final binding free energy is obtained from the average of the 1000 calculated ones.

Names of Proteins	Complexes	MM-GBSA (kcal/mol)
Antioxidant	4IFJ-C14	-20.04
Lung cancer	3VHE-C14	-24.43
Renal	2XIR-C14	-22.40
Breast cancer	3PP0-C14	-21.14

4. Discussion

The phytochemical screening tests of *C. digyna* fruit extracts revealed a diverse set of chemicals. Alkaloids, steroids, flavonoids, glycosides, saponins, tannins, resins, and anthraquinone were found in all

extracts (**Table S1)**, but only the PCDF extract does not contain glycosides. A plant-based diet is known to help prevent many diseases since plants have a huge reservoir of phytochemicals such as flavonoids, alkaloids, saponins, and other polyphenolic substances [47]. The alkaloid compound has been utilized for antibacterial, antiviral, antiprotozoal, and anticancer purposes and has been shown to have fatal effects on breast and colon cancer cells. In addition, tannins' anti-inflammatory, cardioprotective, and antibacterial qualities make them crucial in a variety of biological applications [48]. Plant-derived steroids, on the other hand, are well known for their cardiotonic, antimicrobial, and insecticidal properties. Because of their well-known biological roles, they are frequently employed in medicine [49]. *C. digyna* can be used to treat coronary disorders because it is a source of cardiac glycosides. *C. digyna* plant extracts have an abundance of phytochemicals, which are often employed for their therapeutic advantages.

In qualitative analysis, gas chromatography and mass spectrometry (GC-MS) can deliver more accurate information [50]. Gas chromatography-mass spectra of the ethyl acetate extract showed 40 peaks, demonstrating the existence of 40 distinct phytochemical constituents. **Table S2** displays the compounds' retention time, molecular formula, weight, area, class, and biological activities. The Trimethylsilyl ether of glycerol (C1) compound is a silylated ether class with molecular formula $C_{12}H_{32}O_3Si_3$ that has antioxidant, antibacterial, antifungal, nematocidal, and pesticidal properties [43]. The 1-Methylbenzo[f]quinolin-3-ol (C8) is a quinoline class compound, and it has antimicrobial [51] anticancer, antimalarial, anthelmintic [52] antioxidant and anti-inflammatory effects [53]. The 1,3-Dihydroxyanthraquinone (C14) is a class of anthraquinone that has anticancer [54] and antibacterial [55] effects. In addition, almost all chemicals have different pharmacological activities, except for a few compounds that have not been reported. The 2-(Acetoxymethyl)-3-(methoxycarbonyl) biphenylene was the last phytochemical, with a retention time of 30.538 min and a biphenylene class.

Phenols are essential plant components [56]. Because different plant species' phenolic hydroxyl groups can scavenge free radicals, their total phenol content and antioxidant activity are linearly associated [57]. Flavonoids are divided into flavanones, flavones, isoflavones, flavanols, catechins, anthocyanidins, and chalcones based on their chemical makeup [56]. It has been utilized in preparations for anti-aging, anti-inflammatory, anti-diabetic, and antibacterial purposes. According to earlier studies, plant phenolic compounds may serve as natural antioxidants. Due to their potential biological properties as antioxidants, antiestrogenic, anti-inflammatory, immunomodulatory, cardioprotective, and anti-carcinogenic chemicals, flavonoids and phenols have attracted special attention [48]. Table 1 depicts the TPC and TFC of all extracts, given as MCDF (204.96 ± 4.00 mg GAE/g and 88.14 ± 4.81 mg QCE/g), PCDF (87.01 ± 1.11 mg GAE/g and 38.14 ± 12.73 mg QCE/g), DCDF (215.85 ± 7.28 mg GAE/g, and 115.92 ± 8.33 mg QCE/g, ECDF (258.16 ± 4.84 mg GAE/g and 174.25 ± 8.33 mg QCE/g) and WCDF (233.80 ± 5.88 mg GAE/g and 146.47 ± 12.73 mg QCE/g). *C. digyna* may be a potent medicinal agent for treating a range of illnesses since it can act as a great source of phenols and flavonoids.

The total antioxidant capacity (TAC) was calculated based on the extract conversion of Mo(VI) to Mo(V) and the production of a green phosphate/Mo(V) complex at an acidic pH. It assesses the entire

antioxidant capacity, which takes into account both lipid-soluble and water-soluble antioxidants [58]. By scavenging, accelerating, or preventing the formation of free radicals, antioxidants shield cells from destruction [59]. Among the extracts tested, ECDF exhibited the highest TAC (303.84 ± 8.11 mg/g AAE/g), while PCDF showed the lowest TAC (166.72 ± 6.19 mg/g AAE/g) (Table 1). The absorbance order of AA, MCDF, PCDF, DCDF, ECDF, and WCDF in this situation was AA > ECDF > WCDF > DCDF > MCDF > PCDF.

DPPH is a stable free radical that can receive an electron or a hydrogen radical to form a stable diamagnetic molecule. Antioxidants' ability to scavenge DPPH radicals is assumed to be a result of their hydrogen-donating properties. As a result, DPPH is widely employed to gauge an antioxidant's ability to neutralize free radicals [60]. The absorbance of the reaction mixture dramatically lowered, demonstrating that the chemical under test has a strong potential to scavenge free radicals [61]. The AA and the extracts, in a concentration-dependent manner, inhibited the DPPH radicals. The most effective DPPH radical inhibitory agents were AA (5.27 ± 0.94 µg/mL) > ECDF (10.96 ± 2.32 µg/mL) > WCDF (22.55 ± 2.58 µg/mL) > DCDF (41.61 ± 2.66 µg/mL) > MCDF (57.9 ± 6.87 µg/mL) > PCDF (119.51 ± 6.89 µg/mL) (Table 1).

A common method for assessing a plant's antioxidant capacity is the reducing power [25]. The ability of a molecule to decrease other compounds is a crucial sign of its potential antioxidant effect. Numerous processes have been connected to antioxidant activity, including preventing chain initiation, binding of transition metal ion catalysts, peroxide breakdown, preventing hydrogen abstraction, reductive capacity, and radical scavenging. Antioxidant activity has been connected to the phenomenon of power reduction [62]. Here, ECDF has the highest activity of all extracts since it has the lowest EC_{50} (12.89 ± 1.68 µg/mL). It has been shown that the antioxidant power increases as the EC_{50} value decreases. The FRP's hierarchy was as follows: AA > ECDF > WCDF > DCDF > MCDF > PCDF (Table 1).

Molecular docking approaches have become increasingly popular in recent years, mostly for predicting ligand-target interactions and learning more about the physiologically active molecules found in natural components. It is a common and efficient method for identifying protein-ligand interaction sites, which is essential for identifying hits, optimizing leads, and determining the type of drug-receptor protein interaction [30]. Regarding antioxidant activity, C12 depicts the best binding score (-9.3 kcal/mol) and C7 the worst (-4.5 kcal/mol) with the receptor protein. In contrast, AA has a -6.3 kcal/mol binding affinity with the same protein. For the remaining compounds, the binding affinity ranges from − 4.6 to -8.7 kcal/mol. Molecular docking, nonbonding interaction (2D view), and H-bond surface area of AA (cyan), C14 (magenta), C8 (red), and C12 (blue) compounds with the antioxidant protein are shown in **Figure S2**. Drug stability must be maintained through non-covalent interactions to change binding affinities and boost therapeutic efficacy [44]. Except for C1, C7, and C9 compounds, all the compounds in our investigation contain H-bonds with various amino acids. The C14 has seven H-bonds, two π-alkyl bonds, and six Van Der Waals interactions with numerous amino acids. Moreover, all the drug candidates relate to various hydrophobic bonds such as alkyl, π-alkyl, π-cation, π-σ, π-π-stacked, and π-π-T-shaped. Only AA, C3, and C11 have no hydrophobic bonds.

In this study, we discovered that the A-549 human lung cancer cell line may be considerably inhibited in its development by the DCDF, ECDF, and WCDF extracts of *C. digyna* fruit at doses of 200 µg/mL, 400 µg/mL, and 800 µg/mL (Figs. 4 and 5). The extracts greatly reduced the growth of A-549 cells in a dose-dependent manner. Here, in **Table S4**, the ECDF fraction at doses of 800 µg/mL effectively showed the viability of the lung cancer cell (43.97 ± 2.95%), as compared to the DCDF (63.24 ± 2.36%) and WCDF 65.03 ± 3.57%).

Computational studies against lung cancer proteins (Table 3 and S5) show that C14 had the greatest binding score (-9.2 kcal/mol) in our investigation when compared to other drugs. Here, **Figure S3** depicts molecular docking, nonbonding interaction (2D view), and hydrogen bond surface area of DR (red), C14 (magenta), C8 (orange), and C12 (black) compounds with lung cancer protein 3VHE. The nonbonding interactions revealed eight compounds (C2, C3, C4, C6, C8, C10, C11, C12, C13, and C14) that have H-bonds with various amino acid residues at several distances. Besides, all the molecules exhibit Van Der Waals interactions with amino acid residues, while C3 and C4 compounds do not contain any hydrophobic interactions.

The Vero cell line was exposed to a dose-dependent cytotoxic effect by the DCDF, ECDF, and WCDF extracts. According to the study, healthy cells were unaffected by the extracts, whereas cancer cells were caused to undergo apoptosis. According to **Table S6**, the percentages of Vero cell viability caused by ECDF (800 µg/mL) and WCDF (800 µg/mL) had significant effects with 53.58 ± 3.20% and 56.68 ± 3.98%, respectively.

The outcomes of docking simulation and nonbonding contacts for the renal protein 2XIR are shown in Table 4, S7, and **Figure S4**. In our research, C14 displayed the greatest binding score (-8.8 kcal/mol) with the protein compared to the drug candidates. **Figure S4** shows molecular docking, nonbonding interaction (2D view), and hydrogen bond surface area of DR (red), C14 (blue), C8 (orange), and C12 (magenta) compounds with renal protein. This research demonstrated that, except for C7, C9, C12, C13, and C15, all the selective compounds contain H-bonds with numerous amino acid residues at different distances. The selected compounds have hydrophobic (without C1, C3, C4, and C5) and Van Der Waals bond interactions.

Two breast cancer cell lines (MCF-7 and MDA-MB-231) were used to observe the antiproliferative effects of different concentrations (3.9–500 µg/mL) of formulations of ECDF, as a growth-inhibiting study utilizing MTT-based viability assays. The MTT assay is based on mitochondrial activity. The effect of ECDF extract on MCF-7 and MDA-MB-231 breast cancer cell lines after 72 h stimulation is shown in **Table S8** and Figs. 8 and 9. It can be observed that at the lowest dose tested (3.9 µg/mL), the extract produced a significant increase in cell viability of 90.06 ± 0.72% and 82.98 ± 3.28% for MCF-7 and MDA-MB-231 cell lines. Only at the highest doses (500 µg/mL) tested was a decrease in cell viability noticed for cells 9.17 ± 0.62% (for MCF-7) and 21.09 ± 2.45% (for MDA-MB-231). The results obtained indicate that ECDF extract is rich in phytocompounds with anticancer potential.

Table 5 and S9 and **Figure S5** showed the results of molecular docking experiments and non-bonding interaction investigations against the breast cancer protein. The C14 had the greatest binding score (-9.2 kcal/mol) in our investigation when compared to other drugs with the receptor protein 3PP0. **Figure S5** indicates the molecular docking, nonbonding interaction (2D view), and hydrogen bond surface area of DR (green), C14 (red), C8 (magenta), and C12 (black) compounds with breast cancer protein 3PP0. Herein, the C9, C10, and C12 do not contain H-bonds, but others contain H-bonds with various acid residues at different distances. Besides, they have hydrophobic and Van Der Waals interactions with various pocket residues. Only C7 is absent from hydrophobic bonds.

The MD simulation has become a crucial tool today in mimicking real-time biological phenomena, such as macromolecular dynamics on a computational platform, and comprehending the conformational changes in the ligand-protein complex [63]. Our study suggested that the RMSD values of the protein's Cα atoms (black) and the ligand atoms (blue) for the above proteins-C14 ligand complexes (Figs. 10**(B)-12(B))** are stable along the 400 ns MD simulations. Additionally, with the antioxidant protein, the C14 compound forms four H-bonds with VAL418, VAL465, and ILE559 amino acids, whereas ILE559 (2.38 Å) is the most stable interaction with 70% occupancy. (Fig. 11**(A), (C)**, and **(D))**, shows the C14 ligand interacts with two amino acids GLU917 (100%, 1.76 Å) and CYS919 (98%, 1.98 Å) via two strong H-bonds. For the other two proteins (2XIR and 3PP0), the C14 compound represents moderate to weak H-bonds with various amino acid residues at different distances. The MM-GBSA binding free energy results (Table 6) suggest that compound C14 has similar binding free energies with these four protein targets. In comparison among the four protein targets, the 3VHE-C14 complex had the highest stability due to its lowest binding free energy (-24.43 kcal/mol), with the following order: 3VHE-C14 > 2XIR-C14 > 3PP0-C14 > 4IFJ-C14 complex.

5. Conclusion

In summary, this research indicates that *C. digyna* fruit extracts have strong antioxidant, anticancer, and cytotoxic activities. The results of the phytochemical screening revealed that all extracts had high concentrations of alkaloids, flavonoids, saponins, glycosides, tannins, resins, steroids, and anthraquinone. When compared to MCDF and PCDF extracts in our study, the quantitative analysis showed that TPC, TFC, and TAC were highly present in ECDF, WCDF, and DCDF extracts. Additionally, ECDF, WCDF, and DCDF extracts had the highest levels of DPPH radical scavenging effect and ferric-reducing power when compared to others. According to this study, ECDF, WCDF, and DCDF extracts exhibit strong anticancer and cytotoxic effects against lung, breast cancer, and Vero cell lines. Additionally, 40 phytochemicals with antioxidants, anti-inflammatory, anticancer, antibacterial, antifungal, nematocidal, pesticidal, antimalarial, anthelmintic, and other properties were identified in the GC-MS data. The docking results also showed that some of the selected drug candidates had a strong binding affinity for the respective proteins, and they connected to various amino acid residues via H-bonds, Van Der Waals, and non-covalent interactions. The MD simulation results show that compound C14 forms stable complexes with the respective proteins. So, our research suggests that *C. digyna* might be a

potent source to discover a new medicine with antioxidant, anticancer, and cytotoxic effects. However, more research is needed to discover the bioactive compounds with their impacts and mechanisms of action.

Abbreviations

AA
Ascorbic acid
ANOVA
Analysis of variance
DCDF
Dichloromethane extract of *C. digyna* fruit
DFT
Density functional theory
DMEM
Dulbecco's Minimum Essential Medium
DMSO
Dimethyl Sulfoxide
DPPH
2,2-diphenyl-1-picrylhydrazyl
DR
Doxorubicin
ECDF
Ethyl acetate extract of *C. digyna* fruit
FBS
Fetal bovine serum
FRP
Ferric reducing power
FRPT
Ferric reducing power test
HER2
Human epidermal growth factor-2
MCDF
Methanolic extract of *C. digyna* fruit
MD
Molecular dynamics
MIT
3-(4,5-dimethyl-thiazol-2-yl)-2,5-diphenyltetrazolium bromide
NCCS
National Centre for Cell Science

PCDF
Petroleum extract of *C. digyna* fruit
PDB
Protein data bank
RESP
Restricted electrostatic potential
RMSD
Root mean square deviation
TAC
Total antioxidant capacity
TCA
Trichloroacetic acid
TFC
Total flavonoid content
TPC
Total phenol content
WCDF
Water extract of *C. digyna* fruit
VEGFR2
Vascular endothelial growth factor receptor-2

Declarations

Declaration of Competing Interest

The authors declare no conflict of interest.

Author Contribution

Kaniz Fatema: Fruit collection, Extraction, Experimental analysis, Data curation, Statistical analysis, Computational modeling, Writing–original draft, Writing–review & editing, Md. Anamul Haque: Writing–review & editing, Supervision, Investigation, Formal analysis, Data curation, Conceptualization, Jinat Fatema Sharna: Fruit collection, Experimental analysis, Formal analysis, Md Abdul Majed Patwary: Writing–review & editing, Formal analysis, Md Najem Uddin: Anticancer, Mohsin Kazi: GC-MS analysis, Writing–review & editing, Ashok Kumar: Anticancer, Nellore Bhanu Chandar: Molecular Dynamics Simulation, Chang-Guo Zhan: Writing–review & editing, Computational modeling.

Acknowledgments

The authors acknowledge the assistance of the Bangladesh National Herbarium, Mirpur, Dhaka, Bangladesh, for plant identification and voucher specimen number, the Department of Pharmacy, Comilla University, Bangladesh for lab facilities (where all the experiment assays described in this report were performed), the Computer in Chemistry and Medicine Laboratory, Bangladesh for computational support and suggestions, and the Department of Pharmaceutical Sciences, College of Pharmacy, University of Kentucky for molecular dynamics simulation support.

Data Availability

Data will be made available on request which should be addressed to C.-G.Z. (zhan@uky.edu for the computational data or M.A.H. (anamul@cou.ac.bd for the experimental data).

References

1. Yuan, H., Ma, Q., Ye, L. & Piao, G. The traditional medicine and modern medicine from natural products. *Molecules* **21**, 559 (2016).
2. Makinde, E. A., Ovatlarnporn, C., Adekoya, A. E., Nwabor, O. F. & Olatunji, O. J. Antidiabetic, antioxidant and antimicrobial activity of the aerial part of Tiliacora triandra. *South african J. Bot.* **125**, 337–343 (2019).
3. Umesha, S., Marahel, S. & Aberomand, M. Antioxidant and antidiabetic activities of medicinal plants: A short review. *Int. J. Res. Phytochem. Pharmacol.* **3**, 40–53 (2013).
4. Nelson, V. K. *et al.* In vitro anticancer activity of Eclipta alba whole plant extract on colon cancer cell HCT-116. *BMC Complement. Med. Ther.* **20**, 1–8 (2020).
5. Bray, F. *et al.* Global cancer statistics 2022: GLOBOCAN estimates of incidence and mortality worldwide for 36 cancers in 185 countries. *CA. Cancer J. Clin.* **74**, 229–263 (2024).
6. Mukavi, J. W., Mayeku, P. W., Nyaga, J. M. & Kituyi, S. N. In vitro anti-cancer efficacy and phyto-chemical screening of solvent extracts of Kigelia africana (Lam.) Benth. *Heliyon* **6**, (2020).
7. Kumar, A. *et al.* Apoptosis-mediated anti-proliferative activity of Calligonum comosum against human breast cancer cells, and molecular docking of its major polyphenolics to Caspase-3. *Front. Cell Dev. Biol.* **10**, 972111 (2022).
8. Kuzu, B. & Karakuş, F. Natural compounds targeting VEGFRs in kidney cancer: an in silico prediction. *J. Inst. Sci. Technol.* **12**, 1711–1722 (2022).
9. Emon, N. U. *et al.* Biological and computational studies provide insights into Caesalphinia digyna Rottler stems. *Biochem. Biophys. Reports* **26**, 100994 (2021).
10. Patel, D. K., Kumar, R., Laloo, D. & Hemalatha, S. Natural medicines from plant source used for therapy of diabetes mellitus: An overview of its pharmacological aspects. *Asian Pacific J. Trop. Dis.* **2**, 239–250 (2012).

11. Kumar, R., Patel, D. K., Prasad, S. K., Sairam, K. & Hemalatha, S. Antidiabetic activity of alcoholic root extract of Caesalpinia digyna in streptozotocin-nicotinamide induced diabetic rats. *Asian Pac. J. Trop. Biomed.* **2**, S934–S940 (2012).
12. Emon, N. U. *et al.* Antipyretic activity of Caesalpinia digyna (Rottl.) leaves extract along with phytoconstituent's binding affinity to COX-1, COX-2, and mPGES-1 receptors: In vivo and in silico approaches. *Saudi J. Biol. Sci.* **28**, 5302–5309 (2021).
13. Kupchan, S. M. & Tsou, G. Tumor inhibitors. LXXXI. Structure and partial synthesis of fabacein. *J. Org. Chem.* **38**, 1055–1056 (1973).
14. Fatema, K. *et al.* Antioxidant and antidiabetic effects of Flemingia macrophylla leaf extract and fractions: In vitro, molecular docking, dynamic simulation, pharmacokinetics, and biological activity studies. *BioResources* **19**, 4960–4983 (2024).
15. Ahamad, S. R., Al-Ghadeer, A. R., Ali, R., Qamar, W. & Aljarboa, S. Analysis of inorganic and organic constituents of myrrh resin by GC–MS and ICP-MS: An emphasis on medicinal assets. *Saudi Pharm. J.* **25**, 788–794 (2017).
16. Al-zharani, M. *et al.* In Vitro Cytotoxicity Assessment of Abutilon pannosum Chloroform Fraction and Its Phytoconstituents Analysis. *Processes* **11**, 1306 (2023).
17. Wolfe, K., Wu, X. & Liu, R. H. Antioxidant activity of apple peels. *J. Agric. Food Chem.* **51**, 609–614 (2003).
18. Saeed, N., Khan, M. R. & Shabbir, M. Antioxidant activity, total phenolic and total flavonoid contents of whole plant extracts Torilis leptophylla L. *BMC Complement. Altern. Med.* **12**, 1–12 (2012).
19. Brighente, I. M. C., Dias, M., Verdi, L. G. & Pizzolatti, M. G. Antioxidant activity and total phenolic content of some Brazilian species. *Pharm. Biol.* **45**, 156–161 (2007).
20. Brezoiu, A.-M. *et al.* Polyphenols extract from grape pomace. Characterization and valorisation through encapsulation into mesoporous silica-type matrices. *Food Chem. Toxicol.* **133**, 110787 (2019).
21. Prieto, P., Pineda, M. & Aguilar, M. Spectrophotometric quantitation of antioxidant capacity through the formation of a phosphomolybdenum complex: specific application to the determination of vitamin E. *Anal. Biochem.* **269**, 337–341 (1999).
22. Dutta, S. & Ray, S. Comparative assessment of total phenolic content and in vitro antioxidant activities of bark and leaf methanolic extracts of Manilkara hexandra (Roxb.) Dubard. *J. King Saud Univ.* **32**, 643–647 (2020).
23. Blois, M. S. Antioxidant determinations by the use of a stable free radical. *Nature* **181**, 1199–1200 (1958).
24. Desmarchelier, C., Novoa Bermudez, M. J., Coussio, J., Ciccia, G. & Boveris, A. Antioxidant and prooxidant activities in aqueous extracts of Argentine plants. *Int. J. Pharmacogn.* **35**, 116–120 (1997).
25. Rahman, M., Islam, M., Biswas, M. & Khurshid Alam, A. H. M. In vitro antioxidant and free radical scavenging activity of different parts of Tabebuia pallida growing in Bangladesh. *BMC Res. Notes* **8**,

1–9 (2015).

26. Oyaizu, M. Studies on products of browning reaction antioxidative activities of products of browning reaction prepared from glucosamine. *Japanese J. Nutr. Diet.* **44**, 307–315 (1986).
27. Wilson, C. H. *et al.* Steatosis inhibits liver cell store-operated Ca2+ entry and reduces ER Ca2+ through a protein kinase C-dependent mechanism. *Biochem. J.* **466**, 379–390 (2015).
28. Robinson, J. P., Suriya, K., Subbaiya, R. & Ponmurugan, P. Antioxidant and cytotoxic activity of Tecoma stans against lung cancer cell line (A549). *Brazilian J. Pharm. Sci.* **53**, e00204 (2017).
29. Kazi, M. *et al.* Oral bioactive self-nanoemulsifying drug delivery systems of remdesivir and baricitinib: a paradigmatic case of drug repositioning for cancer management. *Molecules* **28**, 2237 (2023).
30. Fatema, K. *et al.* In-vitro antioxidant and antidiabetic effects of Rorippa indica (L.) extract and fractions with molecular docking, dynamics simulation, ADMET, and PASS studies. *J. Mol. Struct.* 138868 (2024) doi:https://doi.org/10.1016/j.molstruc.2024.138868.
31. Rose, P. W. *et al.* The RCSB protein data bank: integrative view of protein, gene and 3D structural information. *Nucleic Acids Res.* gkw1000 (2016).
32. Gonçalves, A. C., Falcão, A., Alves, G., Silva, L. R. & Flores-Félix, J. D. Antioxidant activity of the main phenolics found in red fruits: An in vitro and in silico study. *Food Chem.* **452**, 139459 (2024).
33. Oguro, Y. *et al.* Design, synthesis, and evaluation of 5-methyl-4-phenoxy-5H-pyrrolo [3, 2-d] pyrimidine derivatives: novel VEGFR2 kinase inhibitors binding to inactive kinase conformation. *Bioorg. Med. Chem.* **18**, 7260–7273 (2010).
34. Karabacak Atay, Ç., Dilek, Ö., Tilki, T. & Dede, B. A novel imidazole-based azo molecule: synthesis, characterization, quantum chemical calculations, molecular docking, molecular dynamics simulations and ADMET properties. *J. Mol. Model.* **29**, 226 (2023).
35. Aertgeerts, K. *et al.* Structural analysis of the mechanism of inhibition and allosteric activation of the kinase domain of HER2 protein. *J. Biol. Chem.* **286**, 18756–18765 (2011).
36. Madhavi Sastry, G., Adzhigirey, M., Day, T., Annabhimoju, R. & Sherman, W. Protein and ligand preparation: parameters, protocols, and influence on virtual screening enrichments. *J. Comput. Aided. Mol. Des.* **27**, 221–234 (2013).
37. Release, S. 4: Maestro, Schrödinger, LLC, New York, NY, 2017. *Google Sch. There is no Corresp. Rec. this Ref.* (2017).
38. Liu, Y. *et al.* CB-Dock2: improved protein–ligand blind docking by integrating cavity detection, docking and homologous template fitting. *Nucleic Acids Res.* **50**, W159–W164 (2022).
39. KB, D. A. C. *et al.* AMBER 2020. *Univ. California, San Fr.* (2020).
40. Frisch, M. J. *et al.* Gaussian 16, revision a. 03, gaussian, inc., wallingford ct. *Gaussian16 (Revision A. 03)* (2016).
41. Cieplak, P., Cornell, W. D., Bayly, C. & Kollman, P. A. Application of the multimolecule and multiconformational RESP methodology to biopolymers: Charge derivation for DNA, RNA, and

proteins. *J. Comput. Chem.* **16**, 1357–1377 (1995).

42. Jorgensen, W. L., Chandrasekhar, J., Madura, J. D., Impey, R. W. & Klein, M. L. Comparison of simple potential functions for simulating liquid water. *J. Chem. Phys.* **79**, 926–935 (1983).
43. Gołębiowski, M. *et al.* The antifungal activity of the cuticular and internal fatty acid methyl esters and alcohols in Calliphora vomitoria. *Parasitology* **140**, 972–985 (2013).
44. Patil, R. *et al.* Optimized hydrophobic interactions and hydrogen bonding at the target-ligand interface leads the pathways of drug-designing. *PLoS One* **5**, e12029 (2010).
45. Alharbi, Y. T. M. *et al.* Investigation of phytochemicals isolated from selected Saudi medicinal plants as natural inhibitors of SARS CoV-2 main protease: In vitro, molecular docking and simulation analysis. *Saudi Pharm. J.* **32**, 102023 (2024).
46. Ahmed, S. *et al.* Molecular docking and dynamics simulation of natural compounds from betel leaves (Piper betle L.) for investigating the potential inhibition of alpha-amylase and alpha-glucosidase of type 2 diabetes. *Molecules* **27**, 4526 (2022).
47. Yao, L. H. *et al.* Flavonoids in food and their health benefits. *Plant foods Hum. Nutr.* **59**, 113–122 (2004).
48. Prasathkumar, M. *et al.* Phytochemical screening and in vitro antibacterial, antioxidant, anti-inflammatory, anti-diabetic, and wound healing attributes of Senna auriculata (L.) Roxb. leaves. *Arab. J. Chem.* **14**, 103345 (2021).
49. Iqbal, E., Salim, K. A. & Lim, L. B. L. Phytochemical screening, total phenolics and antioxidant activities of bark and leaf extracts of Goniothalamus velutinus (Airy Shaw) from Brunei Darussalam. *J. King Saud Univ.* **27**, 224–232 (2015).
50. Cong, Z., Meiling, Q. & Qinglong, S. GC-MS analysis and antibacterial activity of Piper Beetle Linn leaves against Streptococcus mutans. *J Pharm Biomed Anal* **44**, 464–470 (2007).
51. Antoci, V. *et al.* Benzoquinoline derivatives: A straightforward and efficient route to antibacterial and antifungal agents. *Pharmaceuticals* **14**, 335 (2021).
52. Rajesh, Y. B. R. D. Quinoline heterocycles: synthesis and bioactivity. in *Heterocycles-Synthesis and Biological Activities* (IntechOpen, 2018).
53. Asran, M., El-Helw, E. A. E., Azab, M. E., Ramadan, S. K. & Helal, M. H. Synthesis and Antioxidant Activity of Some Benzoquinoline-Based Heterocycles Derived from 2-((3-Chlorobenzo [f] quinolin-2-yl) methylene) hydrazine-1-carbothioamide. *J. Iran. Chem. Soc.* **20**, 3023–3032 (2023).
54. Malik, M. S. *et al.* Journey of anthraquinones as anticancer agents–a systematic review of recent literature. *RSC Adv.* **11**, 35806–35827 (2021).
55. Amorim, J., Vásquez, V., Cabrera, A., Martínez, M. & Carpio, J. In Silico and In Vitro Identification of 1, 8-Dihydroxy-4, 5-dinitroanthraquinone as a New Antibacterial Agent against Staphylococcus aureus and Enterococcus faecalis. *Molecules* **29**, 203 (2023).
56. Subedi, L. *et al.* Antioxidant activity and phenol and flavonoid contents of eight medicinal plants from Western Nepal. *J. Tradit. Chinese Med.* **34**, 584–590 (2014).

57. Vinson, J. A., Su, X., Zubik, L. & Bose, P. Phenol antioxidant quantity and quality in foods: fruits. *J. Agric. Food Chem.* **49**, 5315–5321 (2001).
58. Aliyu, A. B. *et al.* Free radical scavenging and total antioxidant capacity of root extracts of Anchomanes difformis Engl.(Araceae). *Acta Pol Pharm* **70**, 115–121 (2013).
59. Jannat, N. *et al.* Evaluation of the antioxidant, thrombolytic, and antimicrobial effects of Corchorus aestuans L. leaf extracts: an in-vitro and in-silico study. *South African J. Bot.* **164**, 322–333 (2024).
60. Sánchez-Moreno, C. Methods used to evaluate the free radical scavenging activity in foods and biological systems. *Food Sci. Technol. Int.* **8**, 121–137 (2002).
61. Krishnaiah, D., Sarbatly, R. & Nithyanandam, R. A review of the antioxidant potential of medicinal plant species. *Food Bioprod. Process.* **89**, 217–233 (2011).
62. Kumar, R., Tayade, A., Chaurasia, O. P., Sunil, H. & Singh, S. B. Evaluation of anti-oxidant activities and total phenol and flavonoid content of the hydro-alcoholic extracts of Rhodiola sp. *Pharmacogn. J.* **2**, 431–435 (2010).
63. Sasidharan, S., Gosu, V., Tripathi, T. & Saudagar, P. Molecular Dynamics Simulation to Study Protein Conformation and Ligand Interaction BT - Protein Folding Dynamics and Stability: Experimental and Computational Methods. in (eds. Saudagar, P. & Tripathi, T.) 107–127 (Springer Nature Singapore, 2023). doi:10.1007/978-981-99-2079-2_6.

Figures



Figure 1

The whole plant and fruits of *Caesalpinia digyna.*

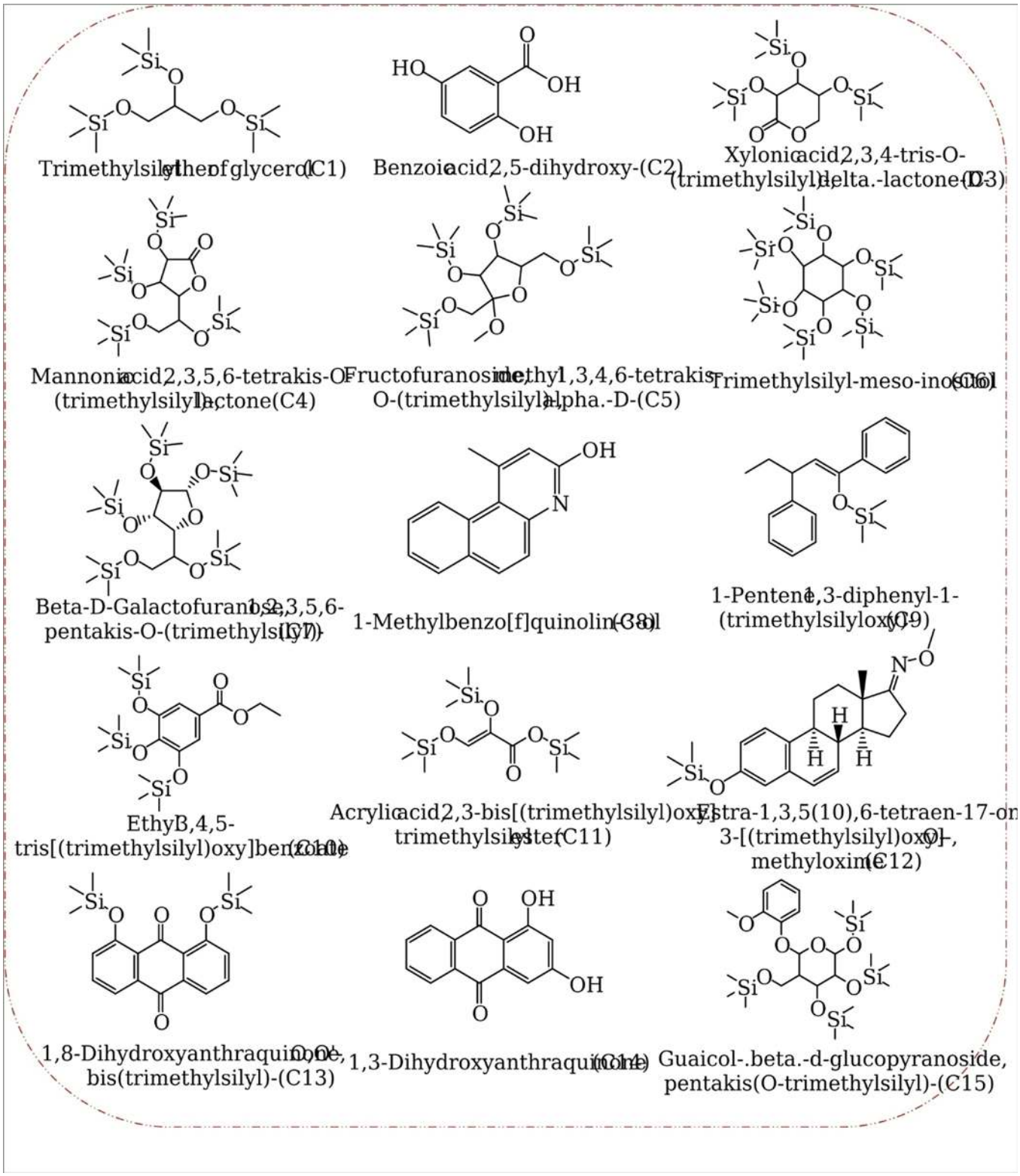


Figure 2

Chemical structures of some selected compounds for computational study.

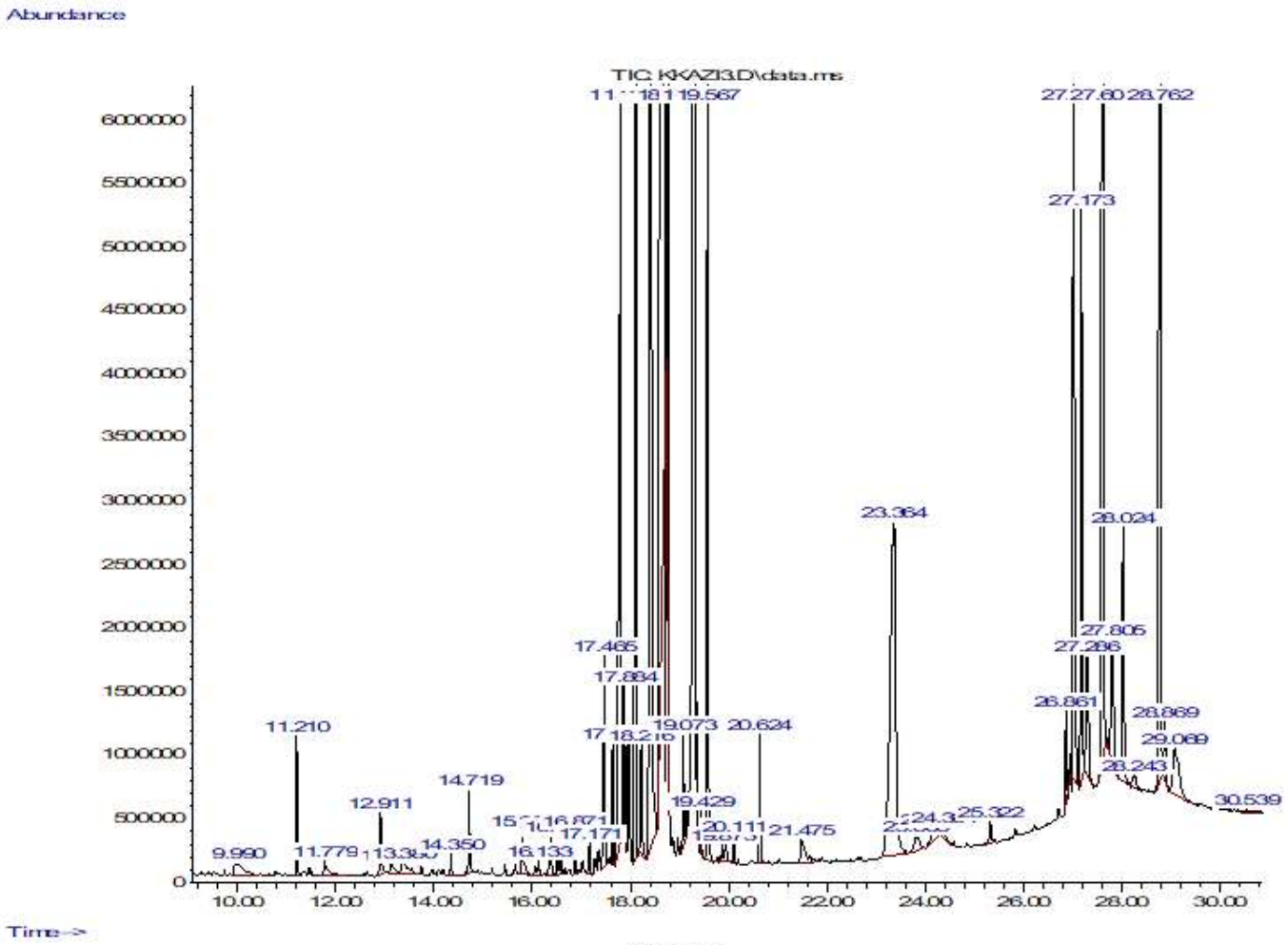


Figure 3

Figure 3

GC–MS chromatogram of the ethyl acetate extract of *C. digyna.*

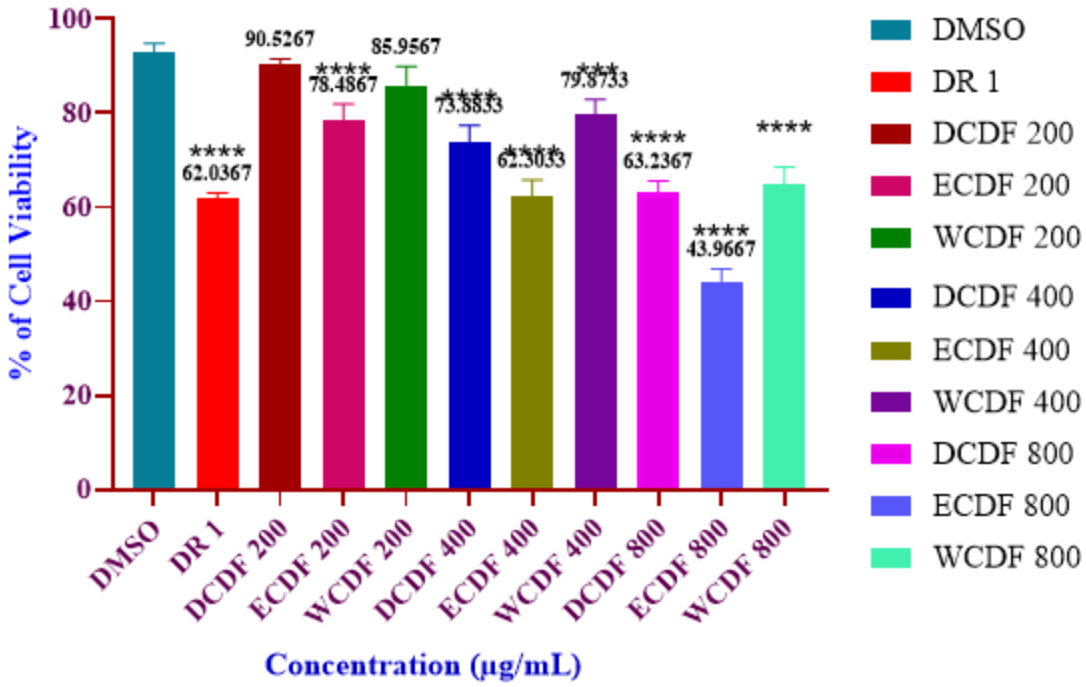


Figure 4

Cell viability (%) of DMSO, DR, and fruit extracts on the lung cancer cell line.

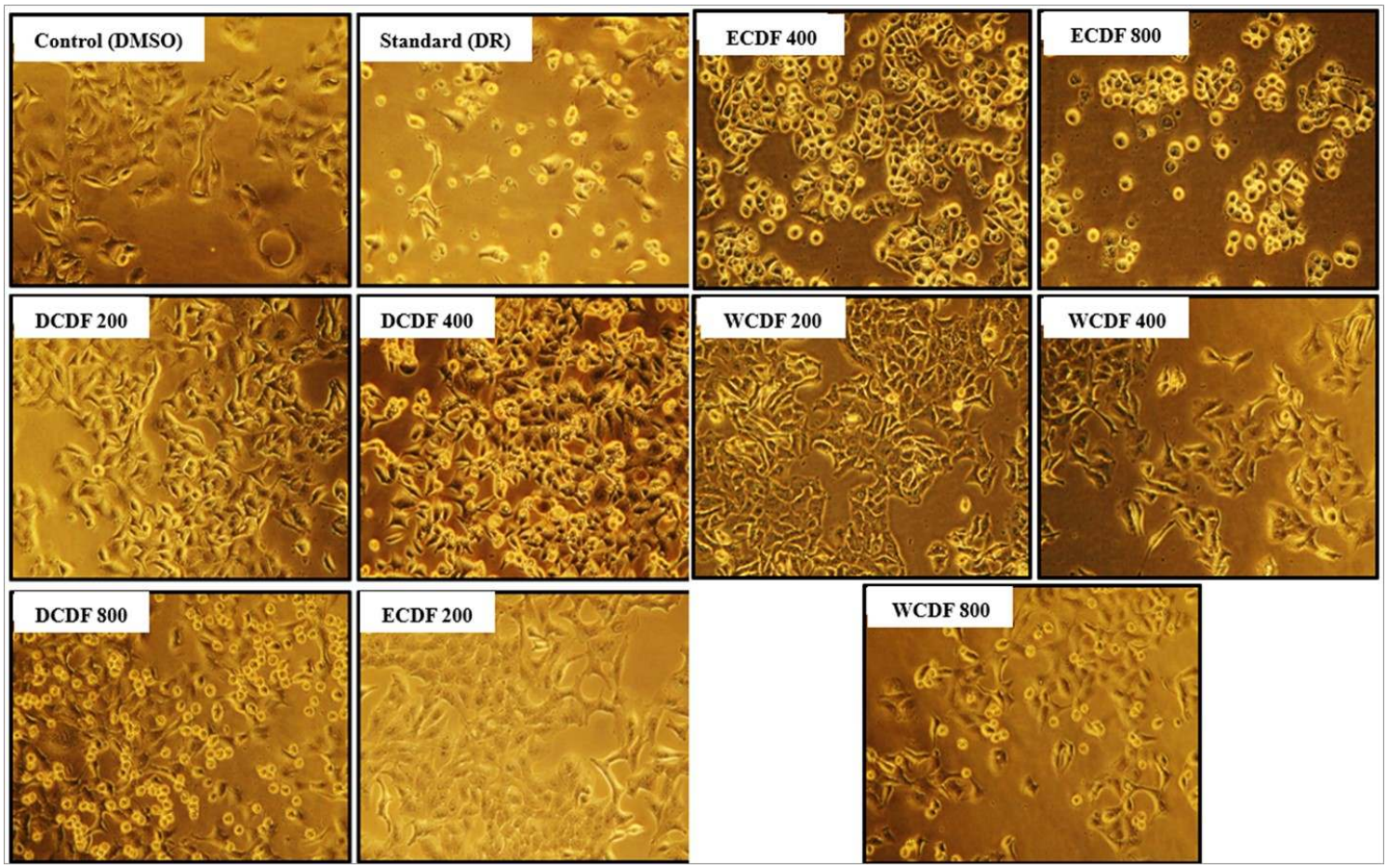


Figure 5

A-549 cell inhibition by DMSO, standard (DR), and fruit extracts.

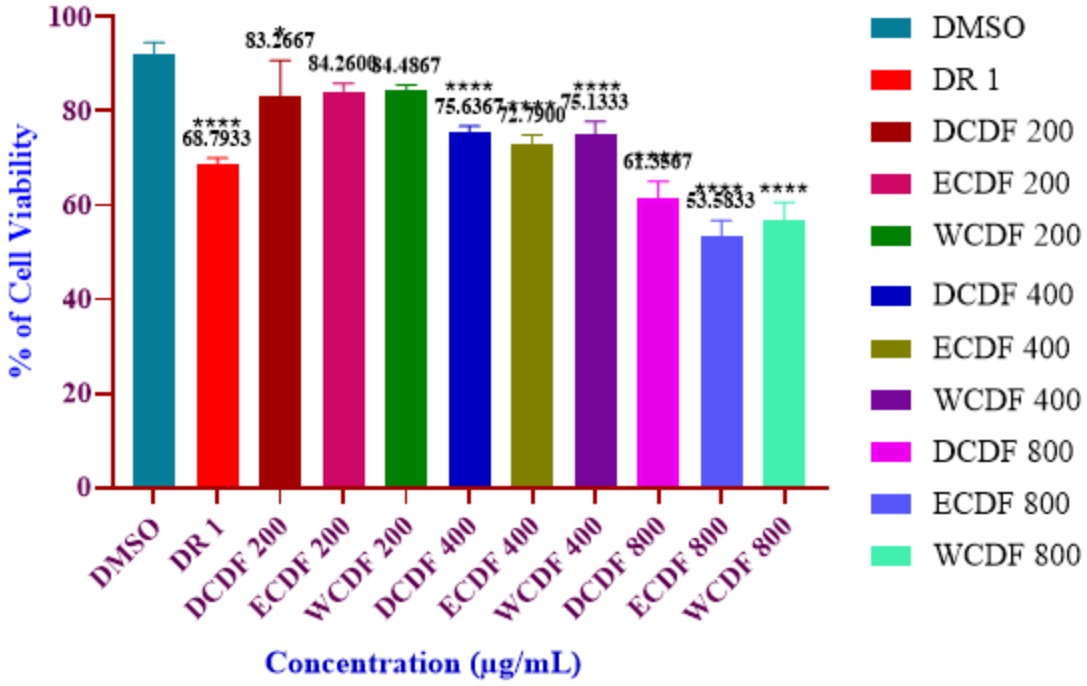


Figure 6

Cell viability (%) of DMSO, DR, and fruit extracts on the Vero cell line.

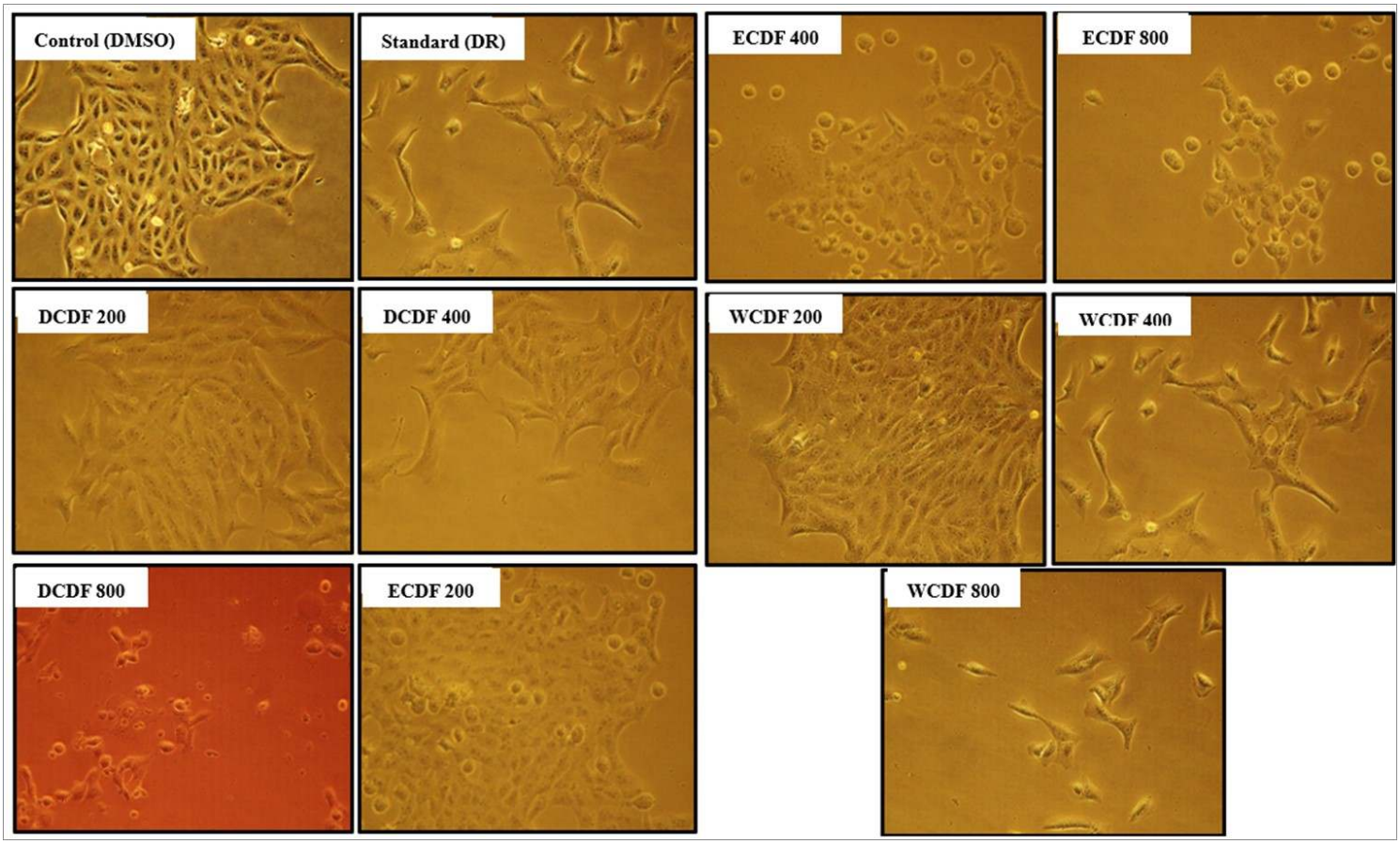


Figure 7

Vero cell inhibition by DMSO, standard (DR), and fruit extracts.

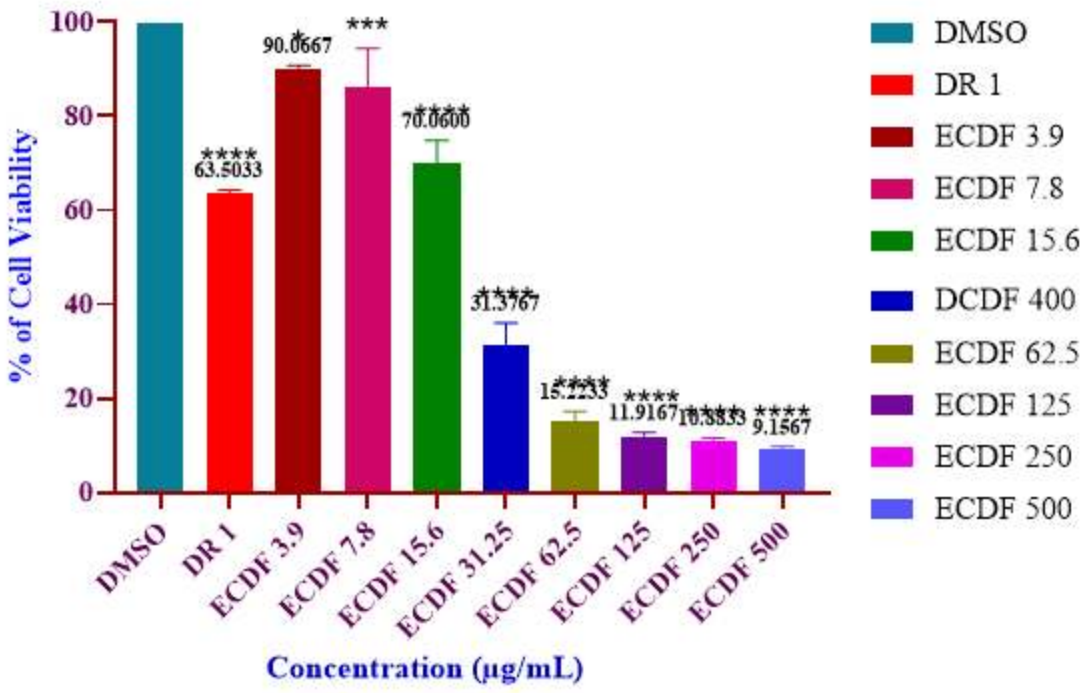


Figure 8

Percentage of cell viability in breast cancer (MCF-7) cell line.

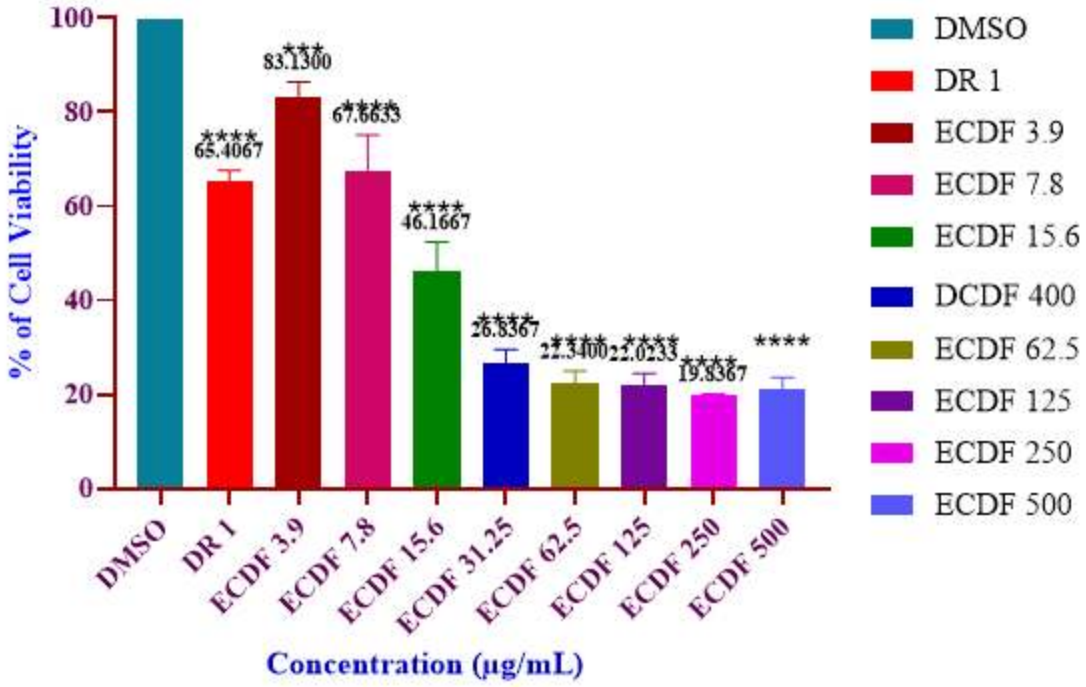


Figure 9

Percentage of cell viability on the breast cancer (MDA-MB-231) cell line.

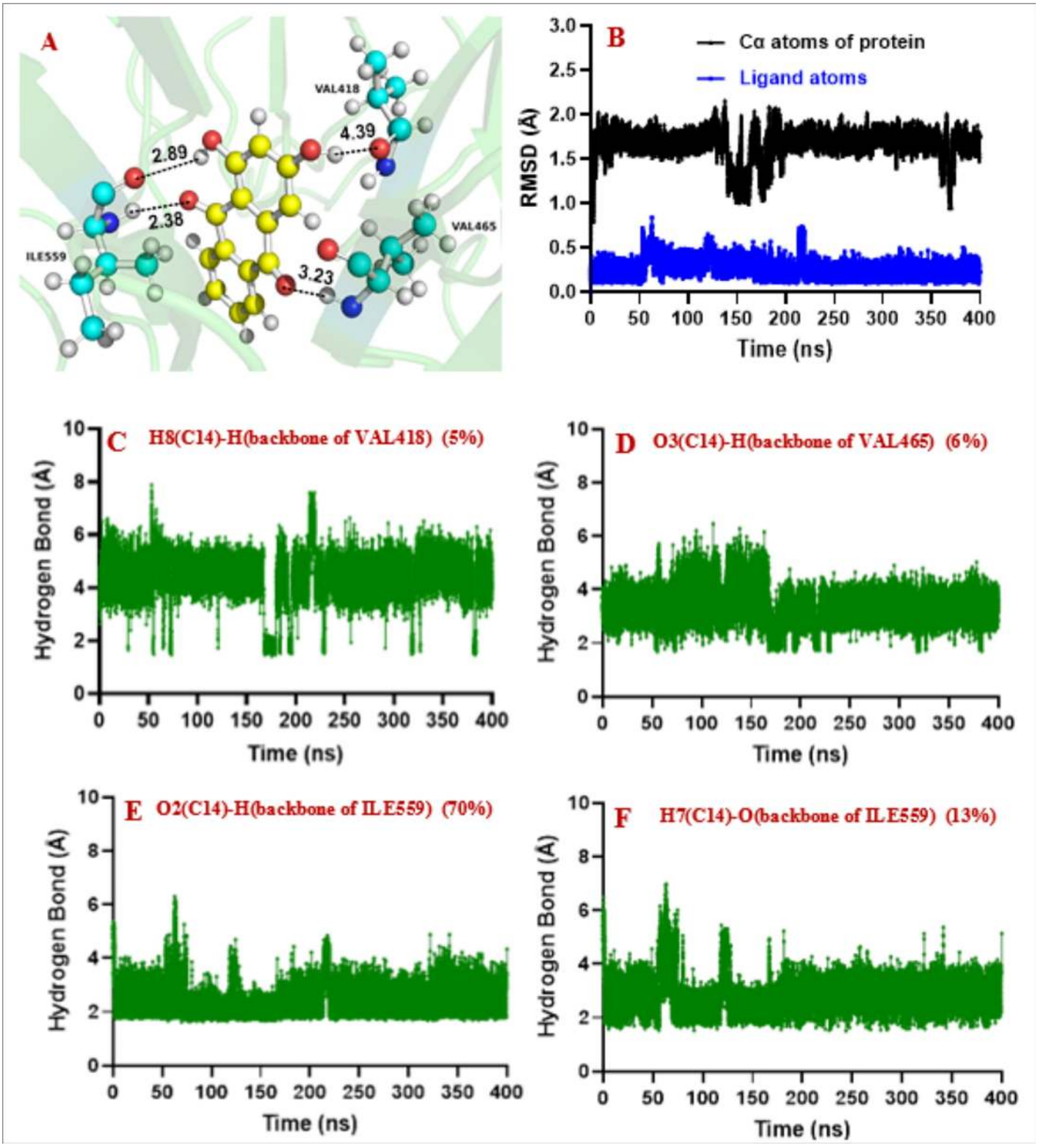


Figure 10

(A) The active site's binding poses of the antioxidant protein (PDB ID: 4IFJ) and C14 ligand are the average distances calculated from the last 100 ns MD simulations. (B) RMSD values for Cα atoms of protein (black) and ligand atoms (blue) during the 400ns MD simulation. Panels (C) to (F) The hydrogen bonding partners' distance from 400 ns and 2.5 cutoff distances percentage in parenthesis from the last 100 ns MD simulations.

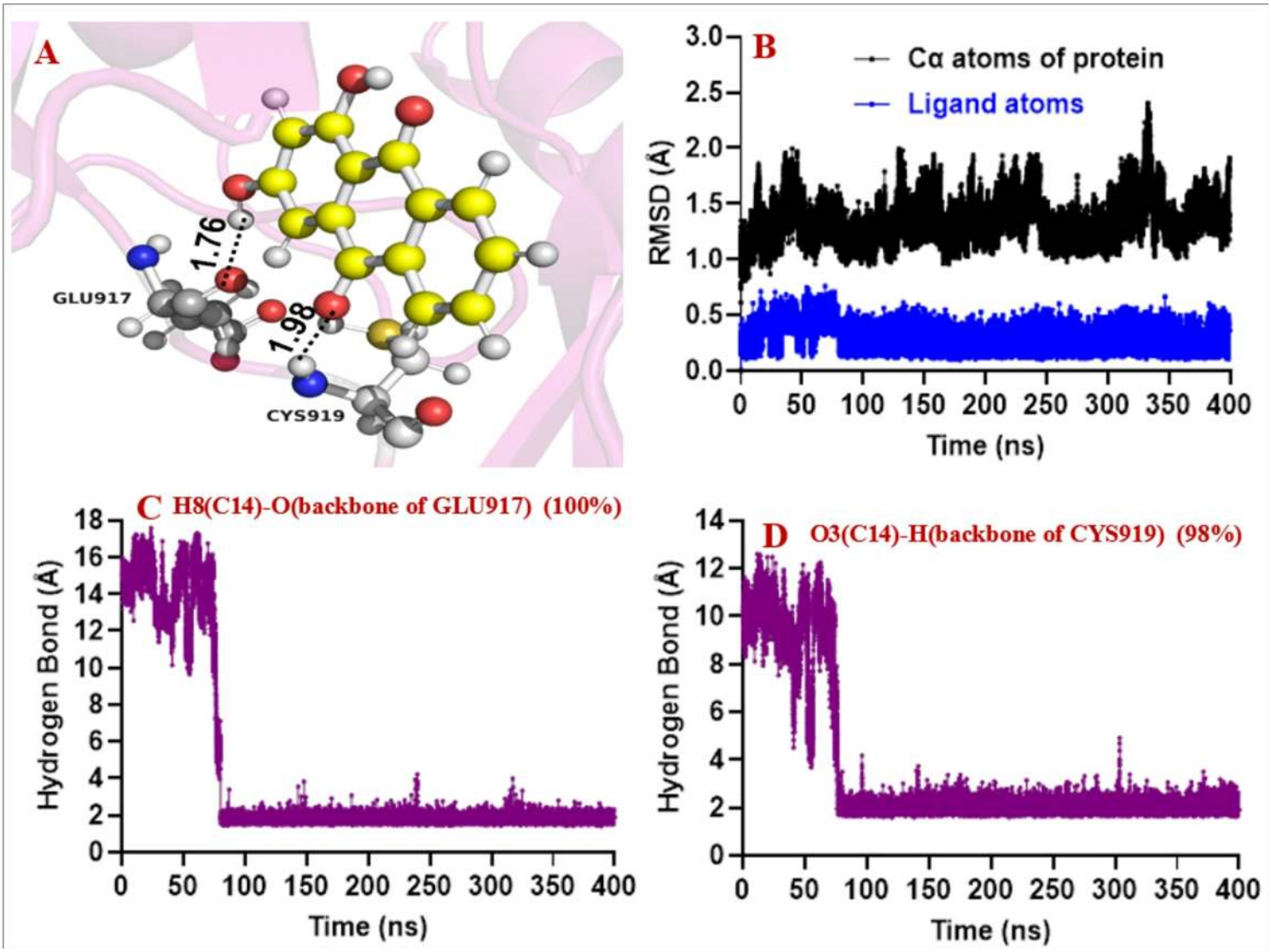


Figure 11

(A) The binding poses of lung cancer protein (PDB ID: 3VHE) and C14 ligand in the active site are the average distances calculated from the last 100 ns MD simulations. (B) RMSD values for Cα atoms of protein (black) and ligand atoms (blue) during the 400 ns simulation. Panels (C) and (D) The hydrogen bonding partners' distances from 400 ns and 2.5 cutoff distances percentage in parenthesis from the last 100 ns MD simulations.

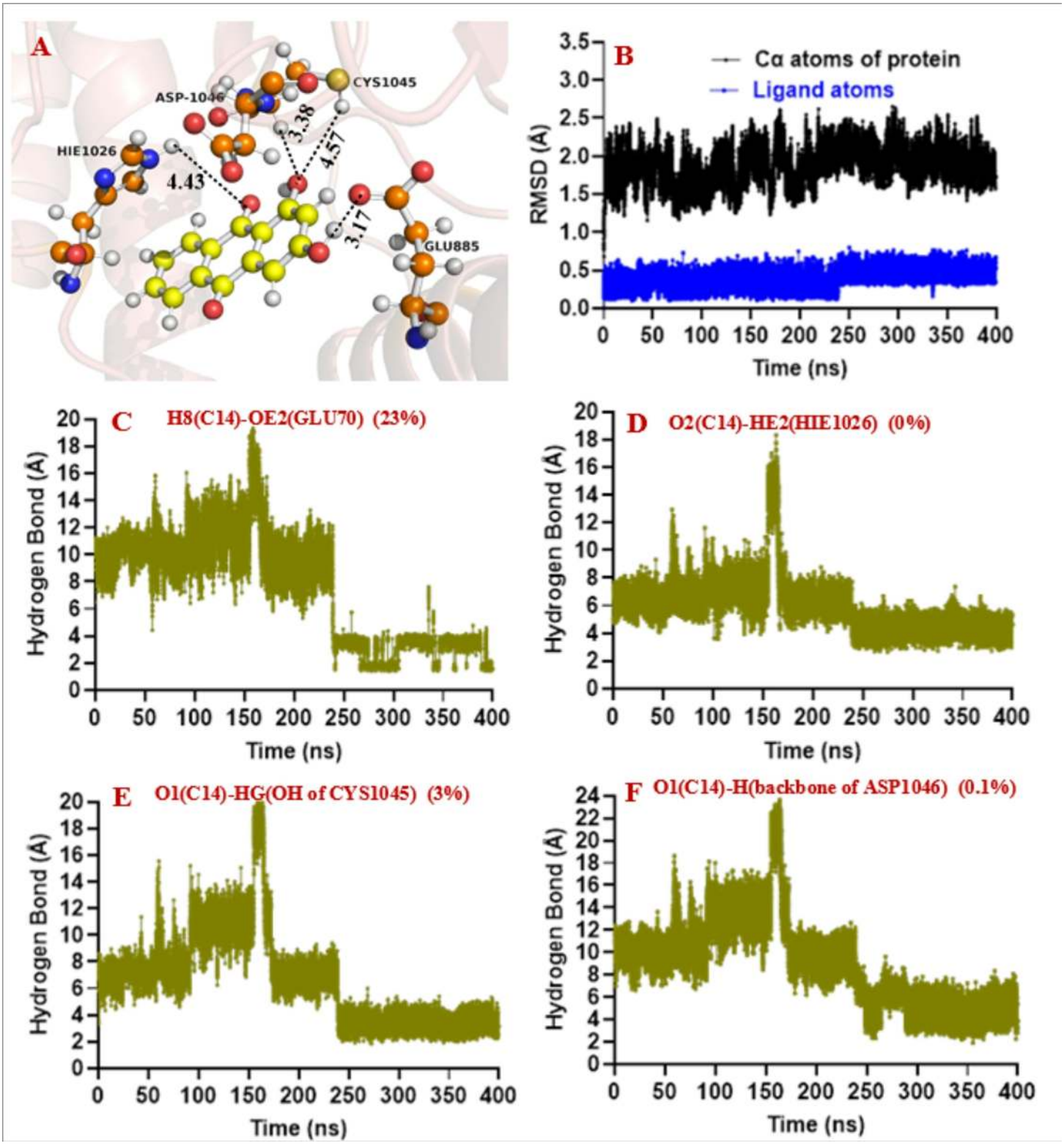


Figure 12

(A) The binding poses of renal protein (PDB ID: 2XIR) and C14 ligand in the active site are the average distances calculated from the last 100 ns MD simulations. (B) RMSD values for Cα atoms of protein (black) and ligand atoms (blue) during the 400 ns simulation. Panels (C) to (F) The hydrogen bonding partners' distances from 400 ns and 2.5 cutoff distances percentage in parenthesis from the last 100 ns MD simulations.

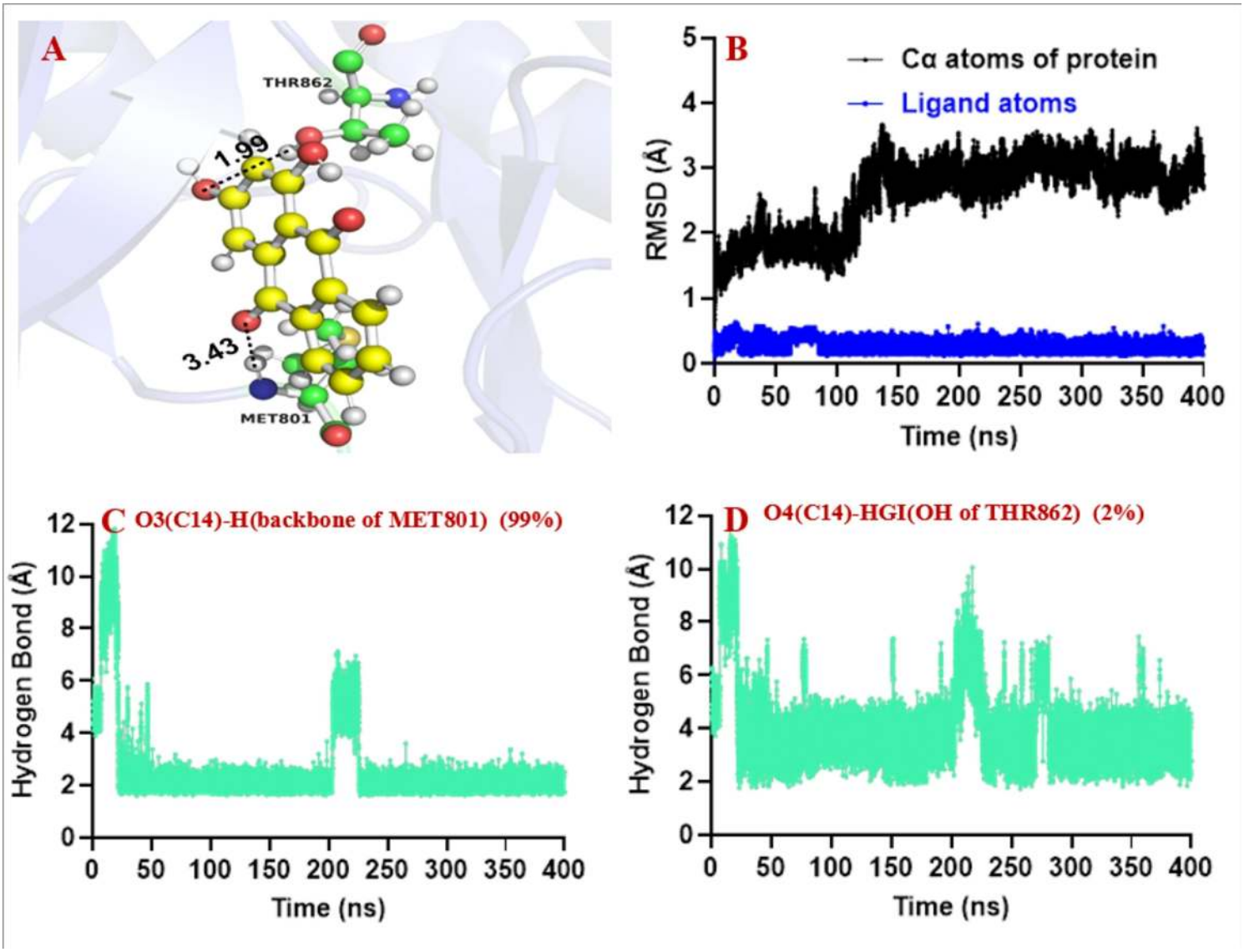


Figure 13

(A) The binding poses of breast cancer protein (PDB ID: 3PP0) and C14 ligand in the active site are the average distances calculated from the last 100 ns MD simulations. (B) RMSD values for Cα atoms of protein (black) and ligand atoms (blue) during the 400 ns simulation. Panels (C) and (D) The hydrogen bonding partners' distances from 400 ns and 2.5 cutoff distances percentage in parenthesis from the last 100 ns MD simulations.

Supplementary Files

This is a list of supplementary files associated with this preprint. Click to download.

- Caesalpiniadigynav3SI.pdf